BNWL-1224
UC-80

3-1
10-69

[redacted]

PLUTONIUM UTILIZATION PROGRAM
TECHNICAL ACTIVITIES QUARTERLY REPORT
JUNE, JULY, AUGUST 1969

October 1969

[redacted]

AEC RESEARCH & DEVELOPMENT REPORT

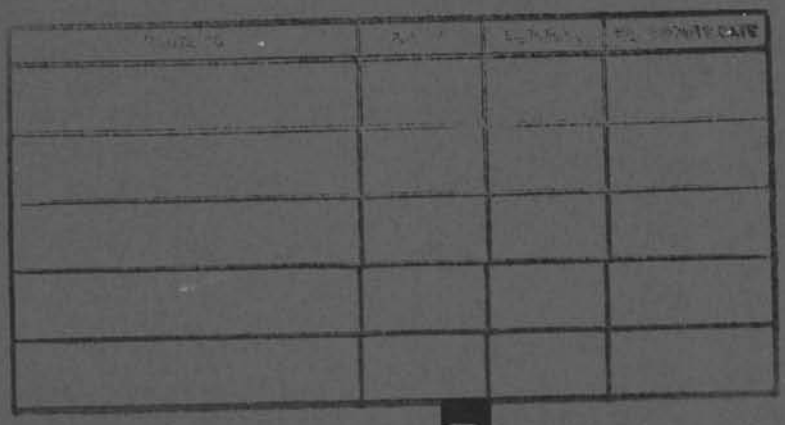

BATTELLE NORTHWEST
BATTELLE MEMORIAL INSTITUTE PACIFIC NORTHWEST LABORATORIES
BATTELLE BOULEVARD, P. O. BOX 999, RICHLAND, WASHINGTON 99352

BNWL-1224

LEGAL NOTICE

This report was prepared as an account of Government sponsored work. Neither the United States, nor the Commission, nor any person acting on behalf of the Commission:

A. Makes any warranty or representation, expressed or implied, with respect to the accuracy, completeness, or usefulness of the information contained in this report, or that the use of any information, apparatus, method, or process disclosed in this report may not infringe privately owned rights; or

B. Assumes any liabilities with respect to the use of, or for damages resulting from the use of any information, apparatus, method, or process disclosed in this report.

As used in the above, "person acting on behalf of the Commission" includes any employee or contractor of the Commission, or employee of such contractor, to the extent that such employee or contractor of the Commission, or employee of such contractor prepares, disseminates, or provides access to, any information pursuant to his employment or contract with the Commission, or his employment with such contractor.

PACIFIC NORTHWEST LABORATORY
RICHLAND, WASHINGTON
operated by
BATTELLE MEMORIAL INSTITUTE
for the
UNITED STATES ATOMIC ENERGY COMMISSION UNDER CONTRACT AT(45-1)-1830

PRINTED IN RICHLAND, WASH.

ERRATA

On page 4.9, the caption of Figure 4.4 should read:

> Measured Axial Power Profile in a TREAT Calibration Capsule (MDF-1) Which Contained an 0.10 in, Thick Hafnium Absorber Disc at Each End of the 5.5 in. Long Enriched UO_2 Fuel Column

The caption for Figure 4.4 as listed in the List of Figures on page viii should also be changed.

BNWL-1224
UC-80, Reactor Technology

PLUTONIUM UTILIZATION PROGRAM
TECHNICAL ACTIVITIES QUARTERLY REPORT
JUNE, JULY, AUGUST 1969

By

Staff of Battelle-Northwest

Program Leader: F. G. Dawson

October 1969

BATTELLE MEMORIAL INSTITUTE
PACIFIC NORTHWEST LABORATORIES
RICHLAND, WASHINGTON 99352

Printed in the United States of America
Available from
Clearinghouse for Federal Scientific and Technical Information
National Bureau of Standards, U.S. Department of Commerce
Springfield, Virginia 22151
Price: Printed Copy $3.00; Microfiche $0.65

PLUTONIUM UTILIZATION PROGRAM

TECHNICAL ACTIVITIES QUARTERLY REPORT

JUNE, JULY, AUGUST 1969

FOREWARD

The Plutonium Utilization Program is conducted by the Pacific Northwest Laboratory for the USAEC. The objective of the Technical Activities Quarterly Report is to inform the scientific community in a timely manner of the technical progress made on the program. The report contains brief technical discussions of accomplishments in all areas where significant progress has been made during the quarter. The results presented should be considered preliminary and do not constitute final publication of the work. A list of publications and papers is given in the report. Anyone wishing to obtain additional information on the work presented is encouraged to contact the author directly.

Since the last quarterly report, major changes have occurred in the Plutonium Utilization Program. Because of funding limitations, the Plutonium Recycle Test Reactor (PRTR) will no longer operate. It is presently being put in a standby condition. The Batch Core Experiment and some fuel experiments that were being conducted in the PRTR will be analyzed and reported during this fiscal year. However, goal fuel exposures were not obtained. Other fuel experiments including defect tests, fission gas release tests and fuel structure characterization tests will be redesigned and will be performed in the ETR and ATR. Future work under the program will emphasize developing the technology on reactor operational and safety characteristics for light water reactors to the extent they are altered or influenced by the addition of recycle plutonium.

PREVIOUS REPORTS IN THIS SERIES

September, October, November 1967	BNWL-654
December 1967, January, February 1968	BNWL-739
March, April, May 1968	BNWL-828
June, July, August 1968	BNWL-907
September, October, November 1968	BNWL-963
December 1968, January, February 1969	BNWL-1039
March, April, May 1969	BNWL-1106

CONTENTS

LIST OF FIGURES

LIST OF TABLES

PLUTONIUM UTILIZATION PROGRAM
TECHNICAL ACTIVITIES QUARTERLY REPORT
JUNE, JULY, AUGUST 1969

1.0 SUMMARY

REACTOR NEUTRONICS

Improvements have been made in the least squares DUBLIK code used for the analysis of burnup data. The improved code has been named BUFIT.

An analytical study was made to determine the sensitivity of calculated values of k_{eff} to the amount of energy and angular detail used in a transport theory solution for a thermal problem. The results show that a 10-group S-8 solution is accurate to within $\pm 0.2\%$ k_{eff}.

Calculations of the fast effect for uranium fueled-H_2O lattices have shown that the error incurred in assuming a homogeneous cell is less than 0.5% in k_{eff}. Thus, if all other sources of error were eliminated in the calculations, we should calculate k_{eff} 1.005 for the UO_2 and the UO_2 - PuO_2 fueled water lattices.

An equivalence approximation has been developed for use in applying the Dunn flux peaking or dipping correction to pin activations.

Destructive analysis data from samples cut from PRTR rods have been received, plotted for consistency checks, and processed through the ISODIL burnup analysis code.

The fourth interim critical tests were conducted on the 55 fuel element Batch Core loading at the PRTR at an average core burnup of 5330 MWd/MTM. Tests were also conducted on two smaller loadings of 31 and 39 fuel elements.

FUELS TECHNOLOGY

Fourteen rods from five elements irradiated in the PRTR core (11,000 MWd/MTM peak) have been selected for detailed examination. Six rods irradiated under the same conditions in the FERTF will also be examined. Visual examination of three of the elements in the basin was completed.

Fourteen rods from nine different type elements irradiated in fringe positions of the PRTR core (18,500 MWd/MTM peak) have been selected for detailed examination. Visual examination of six of the elements was completed in the basin.

Surface dose rate measurements on Yankee (PWR) and Dresden (BWR) high exposure plutonium samples are continuing. Calculations indicate that the dose rate from first generation power reactor plutonium represents a "worst case" situation and the dose rate from plutonium generated in present and planned reactors will be less severe.

A defect testing program will be conducted in the ETR M-3 loop facility at peak linear rod power generations of 20 and 24 kW/ft.

A fuel element assembly instrumented to monitor internal gas pressure within the pellet-containing and vibrationally compacted rods during irradiation will be performed in the ATR. Another fuel assembly instrumented with thermocouples in the fuel will be irradiated in the ETR M-3 loop facility to study in-reactor sintering and grain growth kinetics in pelleted and vibrationally compacted fuel.

REACTOR SAFETY

A comparison was made between the results of burnup calculations obtained using the ZODIAC G and ALTHAEA codes. As a result of this comparison it is concluded that the ALTHAEA code can be used in studies of reactor operation and behavior for plutonium fueled cores as well as uranium fueled cores.

Plutonium loadings for an Oyster Creek assembly have been chosen so that the rod peak-to-average power is less than that in the original uranium-only fuel. Using this reference assembly, the change in reactivity with void fraction was determined for no control, operating temperature conditions.

A joint PNL/GE/INC transient testing program is SPERT has been initiated to study the possible effects of adding PuO_2 enrichment to UO_2 thermal reactor fuels in different ways. Also, transient experiments with cold-pressed-sintered pellet and vibrationally compacted powder fuels will be conducted in the transparent vessel in TREAT to confirm the results of previous tests with the different fuel types.

PRTR

During June, the primary system was filled with heavy water and hydrostatically pressure tested at 1875 psig. The P-4 valve acceptance tests were completed and the reactor was loaded with fifty-five 2 wt% PuO_2 in UO_2 fuel element. The fourth in a series of interim critical tests were conducted with consecutive tests of fifty-five, thirty-one and nineteen fuel elements in a central core array. At the completion of the critical tests, the reactor was de-fueled and preparations begun to drain the systems containing heavy water.

On June 25, 1969, the AEC-RDT approved the preliminary plans for deactivating the PRTR. Work continued throughout the balance of the quarter in draining and drying the coolant systems and deactivating the reactor equipment.

2.0 REACTOR NEUTRONICS

PROGRAM BUFIT: A LEAST SQUARES CODE FOR THE ANALYSIS OF BURNUP DATA

R. P. Matsen

Major changes have been made to the least squares code which is used to extract one group cross section information from isotopic concentration burnup data. The resulting new programs are called BUFIT (burnup fitting code) and DBUFIT, a double precision version. They replace the DUBLIK code[1] which was previously used to perform this type of analysis. Both the DUBLIK and BUFIT codes are framed around the LIKELY[2] general least squares code. The changes fall into four categories:

1. An error in subroutine CHANCE has been corrected. This subroutine which is used to form the first and second derivatives of the least square misfit was incorrectly programmed in the DUBLIK code.

2. Improvements have been made in subroutine THEORY which cause the iterative procedure used in BUFIT to approach the least squares minimum in a more direct fashion. The procedure is now less likely to stop at a false saddle type solution. This is brought about by casting the initial isotopic concentrations as parameters instead of being lumped together with the cross-section ratios as constants of integration which were previously used as parameters. This change greatly reduces the correlation between the parameters that are used in the THEORY equations. The net result seems to be a more reliable iterative path to the solution of the least squares burnup problem.

   An additional equation that describes the ^{239}Pu fissions has been included in the THEORY subroutine for U-Pu

systems. This extra equation provides a better determination of the capture-to-fission ratio for ^{239}Pu, and again, reduces the effort required to arrive at the least squares best fit. Experimental data for ^{239}Pu fissions is required by the BUFIT program; however, these can be obtained from burnup measurements of the total fissions.

3. The iterative scheme used to arrive at the least squares best fit solution has been altered. The new scheme will not proceed to the next iteration unless it has a lower misfit (Q-value) than does the current iteration. Several step types[3] are used in an attempt to obtain a lower misfit. The parameter changes predicted by a given step type are used to generate a new Q-value. If this Q-value is lower than that of the current iteration, the parameters predicted by the step type are used for the next iteration. If the new Q-value is larger than or equal to the current Q-value, the next type of step is tried. The iterative process continues until either the change in the Q-value is less than one part in 10^5 and the parameter variance-covariance matrix is positive definite, or none of the step types yield a lower Q-value.

   If the change in Q estimated from the matrix step is negative, the sequence of steps that are tried is (1) matrix step, (2) half matrix step, (3) gradient step, (4) one fifth of the gradient step, and (5) one twentieth of the matrix step. If the change in Q that is estimated from the matrix step is positive, it is assumed that the parameter changes indicated by the matrix step are in the wrong direction. Therefore, the parameter changes estimated for the half matrix step are reversed and the resulting Q-value computed. If this reversed half matrix step fails, the gradient and succeeding steps are tried.

This series of step types has performed well in the problems that it has been tested on. In general, the matrix half step and the gradient step (and occasionally the reversed matrix half step) are prominent in bringing the iterative process under the influence of the minimum on the Q-value surface where the matrix step becomes dominant. The guaranteed drop in Q-value from one iteration to the next tends to save time by reducing the numbers of false steps that are taken during the iterative process.

4. A new subroutine has been included in the BUFIT program. It calculates the cross section ratios and their one standard deviation errors from the fitted parameters and their variance-covariance 'matrix.

The single precision BUFIT is a little faster and a little less reliable than the double precision DBUFIT code. The DBUFIT code typically requires 3 seconds per iteration for a uranium-plutonium case including data from six spent fuel samples. Starting with rough initial parameter estimates, it converges to the best fit parameters in from 10 to 25 iterations. The BUFIT and DBUFIT codes have been encoded in FORTRAN V language for use on the UNIVAC-1108 computer. These codes are available upon request.

References

1. G. D. Seybold. User's Aid: Programs LEARN AND LIKELY, BNWL-1057, pp. 37-42. Battelle-Northwest, Richland, Washington, May 1969.

2. B. H. Duane. Maximum Likelihood Nonlinear Correlated Fields (BNW Program LIKELY), BNWL-390. Battelle-Northwest, Richland, Washington, September 1967.

3. D. A. Kottwitz. "Nonlinear Least-Squares Fitting Methods," Reactor Physics Department Activities Quarterly Report, April, May, June 1968, BNWL-887. Battelle-Northwest, Richland, Washington, November 1968.

MULTIPLICATION DEPENDENCE ON ENERGY AND ANGULAR DETAIL IN TRANSPORT THEORY CALCULATIONS

S. R. Dwivedi*

Predicting the leakage from clean, critical assemblies is one of the potential causes of inaccuracy in calculated results.

The results of previous analytical studies on selected thermal reactor systems[1,2] show that a systematic difference in calculated values of k_{eff} occurs using diffusion theory and transport theory. *A priori*, it is expected that transport theory is more accurate and that any differences occurring between diffusion and transport theory results is attributable to inaccuracies in diffusion theory.

The object of this study was to determine the sensitivity of calculated values of k_{eff} to the amount of energy and angular detail used in a transport theory solution for a thermal reactor problem. Two homogeneous spherical, critical reactors[3] were selected for the study to: (1) minimize the approximations associated with reactor geometry, and (2) have a high leakage system. The systems were aqueous plutonium nitrate solutions contained in a stainless steel vessel' with one reactor bare and the other reflected with H_2O. A brief description of the systems are given in Table 2.1.

TABLE 2.1. Description of the Reactors[1]

	Critical Mass, kg	H/Pu, atom ratio	Solution Diameter, ID, cm
Plutonium Nitrate Bare Sphere	1.18	668	38.608
Plutonium Nitrate Reflected Sphere (Reflector thickness = 31.5 cm)	1.17	553	38.608

* *Visiting Scientist from Bhabha Atomic Research Centre, Bombay, India.*

The calculations were performed using the HRG[4] and BATTELLE-REVISED THERMOS[5] codes to compute the multigroup spectra and group constants along with DTF-IV[6] code to calculate the system leakage and multiplication, k_{eff}.

The dependence of k_{eff} on energy group detail was calculated using the S-4 approximation in DTF-IV with different multigroup structures, and the results are presented in Table 2.2. The number of groups was varied from four to twenty with varying group boundaries. The group structures used are shown in Table 2.3.

TABLE 2.2. *Calculated* ***Values of k_{eff} for Different Multi-Group Structures***

Total No. of Groups	No. of Groups in the Energy Range, 10 to 0.1 MeV	k_{eff} (a)	
		Bare Sphere	Reflected Sphere
20	10	1.0179	1.0334
18	8	1.0211	1.0373
12	8	1.0196	1.0349
12	2	1.0246	1.0404
10	6	1.0196	1.0354
8	4	1.0241	1.0404
8	2	1.0255	1.0414
6	2	1.0258	1.0420
4	0	1.0839	1.1059

a. Experimental $k_{eff} = 1.000$

Since the maximum number of groups at high energies is limited by the minimum lethargy width of 0.25 in HRG, the value of k_{eff} obtained from the 20-group calculation can be assumed to be the most accurate. Relative to this value of k_{eff}, it is seen that the multiplication is sensitive to both the number of energy groups and the group structure. From a

practical standpoint, 10-group model with six high energy groups is sufficient, in that k_{eff} is accurate to within ±0.2%. The 10-group model was obtained by arranging the levels in the energy range 0.1 to 10 MeV, such that nearly equal number of fission neutrons are generated in each group, i.e., the fission spectrum is almost constant. It is also seen from the results in Table 2.3 that the multiplication is relatively insensitive to energy detail below this range (i.e., <0.1 MeV).

TABLE 2.3. ***Group Structure (Lower Energy Boundaries in eV)***

20 Groups	18 Groups	12 Groups	10 Groups	8 Groups	6 Groups	4 Groups
7.79×10^6	--					
6.07×10^6	--			--		
4.72×10^6	--		4.72×10^6			
3.68×10^6	--					
2.87×10^6	--		2.87×10^6	--		
2.23×10^6						
1.74×10^6	--		1.74×10^6			
1.35×10^6	--	--	1.35×10^6	--	--	--
4.98×10^5	--		4.98×10^5			
1.83×10^5	--	--	1.83×10^5		--	--
2.48×10^4	--	--	1.17×10^4	--	--	--
3.36×10^3	--	--			--	
4.54×10^2	--	--				
1.01×10^2	--	--			--	
37.3	--	--				
13.7	--	--				
5.04	--	--				
1.86	--	--	2.38	--	--	--
0.683	--	--	0.683	--	--	--
0.0	--	--	0.0	--	--	--

The effects of higher order Sn approximations on the calculated results are presented in Table 2.4. These results show a $\leq$0.04% effect on k_{eff} in going from S-16 to S-8 and a $\leq$0.2% effect in going from S-8 to S-4 independent of number of groups. Thus, it is concluded that a 10-group S-8 calculation is sufficient in accuracy.

TABLE 2.4. Effects of Using Higher Order Sn Approximation

Total No. of Groups	Sn-order	k_{eff} Bare Sphere	k_{eff} Reflected Sphere
20	4	1.0179	1.0334
20	8	1.0154	1.0314
20	16	1.0151	1.0310
10	4	1.0196	1.0354
10	8	1.0171	1.0335
10	16	1.0168	1.0331

A comparison between values of k_{eff} obtained using diffusion theory (HTN) [7] and transport theory is made in Table 2.5. The table shows that diffusion theory gives results which are insensitive to number of groups whereas transport theory results are sensitive. Also, the diffusion theory results agree better with experiment. This conclusion does not indicate that the lower order diffusion theory is more accurate, but probably that compensating errors exist in the calculational modei. It will be interesting to pinpoint those errors and to investigate the region where diffusion theory will not be able to compensate those errors.

TABLE 2.5. Comparison Between Results of Transport Theory and Diffusion Theory Calculations

No, of Groups	Calculational Mode	k_{eff} Bare Sphere	k_{eff} Reflected Sphere
18	Transport	1.0211	1.0373
	Diffusion	1.0140	1.0194
4	Transport	1.0839	1.1059
	Diffusion	1.0133	1.0192

Based upon the results presented here the following conclusions can be drawn:

- Transport theory results are very sensitive to the number of multigroups used to describe the fission spectrum, and the best estimate of k_{eff} can be obtained when the fission spectrum is uniformly distributed in the fast energy groups.
  - a Using the 10-group structure as described in Table 2.3, the value of k_{eff} can be calculated within the accuracy of 0.2% (in comparison to 20-group model).
  - a For high leakage systems as described above, the S-8 approximation is sufficient. S-4 theory overestimates the eigenvalue by 0.2%.
  - a Diffusion theory is insensitive to the number of multigroups used in the high energy region. Compensating errors must exist in the diffusion theory calculations which give better values of multiplication factors than transport theory. These compensatory errors are different from the one customarily encountered, i.e., compensatory errors due to basic cross-sections and spectrum model.
- The most elaborate transport theory calculations overestimate k_{eff} by about 1.5% for the bare system and about 3% for reflected systems. The reasons for these errors are not known; however, the first area to attack seems to be the spatial-spectral model (e.g., perhaps the reflected sphere needs to be described by multiple core and reflector regions with different group constants).

REFERENCES

1. *C. R. Richey. "Theoretical Analysis of Homogeneous Plutonium Critical Experiments," Nucl. Sci. Eng., vol. 31, p. 32. 1968.*

2. *U. P. Jenquin. Unpublished Data. Battelle-Northwest, Richland, Washington. (Private Communication)*

3. R. C. Lloyd, et al. "Criticality Studies with Plutonium Solutions," Nucl. Sci. Eng., vol. 25, p. 165. 1966.

4. J. L. Carter, Jr. "Effective Cross-Sections for Resonances in HRG," and "Computer Code Abstracts," Technical Activities Quarterly Report, July, August, September 1966, BNWL-340. Battelle-Northwest, Richland, Washington. 1966.

5. D. R. Skeen and L. J. Page. THERMOS/BATTELLE: The Battelle Version of the THERMOS Code, BNWL-516. Battelle-Northwest, Richland, Washington, September 2967.

6. K. D. Lathrop. DTF-IV, A Fortran-IV Program for Solving the Multigroup Transport Equation for Anisotropic Scattering, LA-3373. Los Alamos Scientific Laboratory, New Mexico, July 1965.

J. R. Lilley, Jr. Computer Code HFN-Multigroup, Multiregion Neutron Diffusion Theory in One Space Dimension, HW-71545. Available from Clearinghouse for Federal Scientific and Technical Information, Springfield, Virginia, 1961.

HETEROGENEITY CORRECTION TO FAST-FISSIONS

S. R. Dwivedi*

In the analysis of light-water moderated, enriched uranium or plutonium lattices, the fast fission in ^{238}U is usually obtained from multigroup calculations of the fast neutron spectrum of the finite homogenized lattice. In this usual approach one neglects a heterogeneity correction (spatial effect) in the fast energy range. This effect is relatively small because of the long mean free path for neutrons, but it is not negligible. The object of this study was to determine how large an error is introduced in the calculated k_{eff} of typical enriched UO_2 lattices by neglecting the spatial detail. Multigroup calculations for the homogeneous cells were calculated using the HRG code.(1)

The unit cell was assumed to consist of the fuel region and moderator region, and the collision equations were solved using a constant fission source in the fuel region. The

* Visiting Scientist from Bhabha Atomic Research Centre, Bombay, India.

reaction rate in ^{238}U nuclei was obtained using a well known variational principle. The calculations were performed only for neutrons having energies greater than 1.35 MeV.

The neutron balance equation can be written as

$$\Sigma_1^t \phi_1 = \left(\beta\nu\Sigma_1^f + \Sigma_1^s\right) \phi_1 P_{11} + \Sigma_2^s \phi_2 P_{21} + S P_{11}$$

$$\Sigma_2^t \phi_2 = \left(\beta\nu\Sigma_1^f + \Sigma_1^s\right) \phi_1 P_{12} + \Sigma_2^s \phi_2 P_{22} + S P_{12} \qquad (1)$$

where

$\Sigma_i^s = V_i \sum_j N_j \sigma_j^s$

i = 1, 2

j = all the nuclei in region i

V_i = volume fraction of i^{th} region

σ_j^s = microscopic scattering cross-section with neutron energy remaining above 1.35 MeV after scattering

N_j = nuclei density

β = fraction of fission neutrons generated above 1.35 MeV

$\nu\Sigma_i^f = V_i \sum_j N_j \nu_j \sigma_j^f$

$\nu_j u_i$ = number of neutrons generated due to fast fissions in nuclei j

$\Sigma_i^t = \Sigma_i^{rem} + \Sigma_i^s$

$\Sigma_i^{rem} = V_i \sum_j N_j \sigma_i^{rem}$

σ_j^{rem} = removal cross-section of j^{th} nuclei

S = uniformly distributed source in region 1

P_{ij} = probability of a neutron generated uniformly in region i to have its first collision in region j.

Equation (1) can be written in a matrix form as

$$[H]\,[\phi] + [S] = 0,$$

where

$$[H] = \begin{bmatrix} \left(\beta\nu\Sigma_1^f + \Sigma_1^s\right) P_{11} - \Sigma_1^t & \Sigma_2^s P_{21} \\ \left(\beta\nu\Sigma_1^f + \Sigma_1^s\right) P_{12} & \Sigma_2^s P_{22} - \Sigma_2^t \end{bmatrix}$$

$$[\phi] = \begin{bmatrix} \phi_1 \\ \phi_2 \end{bmatrix}$$

$$[S] = \begin{bmatrix} SP_{11} \\ SP_{12} \end{bmatrix}$$

We are interested in the reaction rate in ^{238}U due to the fission source S. If Σ_u^f is the fission cross section of ^{238}U, then the required quantity is

$$\left[\Sigma_u^f,\ 0\right] \times \begin{bmatrix} \phi_1 \\ \phi_2 \end{bmatrix}.$$

The variational principle which can be used to calculate this quantity is given by

$$L\left[\phi,\ \phi^*,\ \Sigma_u^f\right] = [S^*]^T\,[\phi] + [\phi^*]^T\,[H]\,[\phi] + [\phi^*]^T\,[S], \qquad (2)$$

where the superscript T represents the transpose of the matrix and $[\phi^*]$ is the solution of the adjoint equation

$$[H^*]\,[\phi^*] + [S^*] = 0, \qquad (3)$$

where

$$[H^*] = \begin{bmatrix} \left(\beta\nu\Sigma_1^f + \Sigma_1^s\right) P_{11} - \Sigma_1^t & \left(\beta\nu\Sigma_1^f + \Sigma_1^s\right) P_{12} \\ \Sigma_2^s P_{21} & \Sigma_2^s P_{22} - \Sigma_2^t \end{bmatrix}$$

$$[\phi^*] = \begin{bmatrix} \phi_1^* \\ \phi_2^* \end{bmatrix}$$

$$[S^*] = \begin{bmatrix} \Sigma_u^f \\ o \end{bmatrix}.$$

The first order approximation to the direct and adjoint fluxes to be used in equation (2) can be obtained from the solution for the corresponding homogeneous lattice cell. The stationary behavior of the variational principle will cause a second order error in the uranium reaction rate. The neutron balance equation for a homogeneous cell can be formed by substituting P_{ij}^o (the collision probabilities in homogeneous mixture) in place of P_{ij} in equations (1) and (3). The solutions to these equations will be given by

$$\phi_1^o = \phi_2^o = \frac{S}{\Sigma_1^t + \Sigma_2^t - \left(\beta\nu\Sigma_1^f + \Sigma_1^s + \Sigma_2^s\right)}$$

$$\text{and } \phi_1^{*o} \quad \phi_2^{*o} = \frac{\Sigma_u^f \left(\Sigma_i^t + \Sigma_2^t\right)\left(1 - \Sigma_2^s/\Sigma_2^t\right)}{\Sigma_1^t \left(\Sigma_1^t + \Sigma_2^t - \beta\nu\Sigma_1^f - \Sigma_1^s - \Sigma_2^s\right)} \tag{4}$$

where the superscript o represents the homogeneous solution.

Using these values of direct and adjoint fluxes in the variational principle (2) the ratio of reaction rates in ^{238}U nuclei in heterogeneous to the homogeneous case can be given by

$$\gamma = 1 + \delta P_c \left(1 + \frac{\Sigma_2^t}{\Sigma_1^t}\right)^2 \left(1 - \frac{\Sigma_2^s}{\Sigma_2^t}\right)^2 \times \frac{\Sigma_1^t}{\left(\Sigma_1^t + \Sigma_2^t - \beta\nu\Sigma_1^f - \Sigma_1^s - \Sigma_2^s\right)} \tag{5}$$

where δP_c is the difference in first flight collisions in uranium due to the heterogeneity of the lattice.

Using the Glasstone and Edlund[2] definition of ε (the fast-fission factor), the heterogeneity contribution to the eigenvalue can be given by

$$\frac{\Delta k}{k} = \frac{\Delta \varepsilon}{\varepsilon} = \frac{\gamma - 1}{1 + \dfrac{\Sigma_1^t + \Sigma_2^t - \left(\beta \nu \Sigma_1^f + \Sigma_1^s + \Sigma_2^s\right)}{\beta \left(\bar{\nu}_{28} - 1\right) \Sigma_u^f}} \qquad (6)$$

where ν_{28} = average ν for ^{238}U above 1.35 MeV. The following equations were used in deriving equation (6)

$$\delta_{hom}^{28} = \frac{\beta \nu^{25} \Sigma_u^f}{\Sigma_1^t + \Sigma_2^t - \left(\beta \nu \Sigma_1^f + \Sigma_1^s + \Sigma_2^s\right)}$$

$$(\varepsilon - 1)_{hom} = \frac{\bar{\nu}_{28} - 1}{\nu_{25}} \delta^{28}$$

$$\frac{(\varepsilon - 1)_{het}}{(\varepsilon - 1)_{hom}} = \frac{\delta_{het}^{28}}{\delta_{hom}^{28}} = \gamma$$

δ^{28} = fast-fission ratio of ^{238}U

The error in k_{eff} caused by neglecting heterogeneity in the calculation of fast fission in ^{238}U was calculated for five enriched uranium lattices with different moderator-to-fuel volume ratios. The macroscopic cross sections were obtained from HRG,[1] and p_c^{het}, the first flight collision probability with uranium nuclei, was calculated from the following relation given by Nordheim[3]

$$p_c^{het} = 1 - \frac{P_o}{1 + \dfrac{C}{1 - C} \bar{\ell} \Sigma_o P_o}$$

In this equation, C is the Dancoff correction factor calculated with the code DASQHE;[4] $\bar{\ell}$ is the mean chord length in the rod; Σ_o is the macroscopic total cross-section of UO_2; and P_o is the escape probability given by Case, deHoffman and Placzek:[5]

$$P_o(x) = \times \left\{ 2x \left[K_1(x)\, I_1(x) + K_o(x)\, I_o(x) \right] - 2 + \frac{1}{x} K_1(x)\, I_1(x) - K_o(x)\, I_1(x) + K_1(x)\, I_o(x) \right\}$$

where $x = r \cdot \Sigma_o$, r = radius of the rod. The results of the calculations are presented in Table 2.6. The error in k, due to neglecting heterogeneity in the calculation of fast fissions in ^{238}U is always less than 5 mk.

TABLE 2.6. Heterogeneity Corrections to Fast-Fissions

Lattice, Enrichment	Rod Radius, cm	V_m/V_f, Vol. Ratio	γ	$\Delta k/k$, %
(2.734%)	0.389	1.048	1.0353	0.22
(3.037%)	0.5634	1.15	1.0599	0.31
(1.328%)	0.5042	1.43	1.054	0.28
(1.328%)	0.5042	2.40	1.100	0.36
(2.35%)	0.5588	2.41	1.137	0.45

REFERENCES

1. *J. L. Carter, Jr. "Computer Code Abstracts, Computer Code HRG," Reactor Physics Department Technical kctivities Quarterly Progress Report, July, August, September 1966, BNWL-340. Batte Zle-Northwest, Richland, Washington, October 15, 1966.*
2. *Glasstone and Edlund. The Elements of Nuclear Reactor Theory, Van Nostrand Co., Princeton, New Jersey, 1962.*
3. *L. W. Nordheim. Symp. Appl. Math., vol. 11, p. 58. 1961.*
4. *I. Carlvik. "The Dancoff Correction in Square and Hexagonal Lattices," Nucl. Sci. Eng., vol. 29, p. 325. 1967.*
5. *K. M. Case, F. deHoffman, and G. Placzek. Introduction to the Theory of Neutron Diffusion, U. S. Government Printing Office, Washington, D. C., 1953.*

AN EQUIVALENCE APPROXIMATION FOR USE IN APPLYING THE DUNN FLUX PEAKING OR DIPPING CORRECTION TO PIN ACTIVITIES

C. L. Bennett and D. R. Oden

In performing lattice parameter measurements by foil activation techniques, it is important to correct for the peaking or dipping of the flux in the foil with respect to the surrounding media, especially in the thermal energy range. One such method that is both reasonably accurate and simple to apply is the Dunn approximation.[1] This method has been routinely applied to foil (mostly round and square shaped) activities in the analysis of PCTR experiments since about 1967.[2] In addition to the standard foil data in such experiments, extensive pin activation data has usually been obtained also. The usual procedure in the past has been to only use the pin data (uncorrected) for inferring cell spacial shape detail and as backup for the standard foil data. Therefore, in order to increase the usefulness of this data, some sort of a foil peaking or depression correction method was also needed for pin activities.

We decided first to directly apply the Dunn approximation by obtaining an approximate equivalence relationship between finite slabs and cylinders and then possibly at some later date, either take the more obvious direct approach of explicitly deriving a first order pin correction or use some other more accurate correction method.

First, this note briefly outlines the Dunn approximation, then presents the determination of the approximate equivalence relationships (actually two are involved) required to apply the correction to pins, and finally it summarizes the resulting procedure for actually using this method.

The Dunn Approximation

If A is the activation of a square or round foil of thickness t and A_o is the activation that would occur if the flux in the foil were the same as in the surrounding medium then Dunn's approximation can be written as

$$\frac{A_o}{A} = 1 + \left(\Sigma_a^{med.} - \Sigma_a^{foil}\right) t \ln \frac{\beta}{t},$$

$$\beta = \begin{cases} L(\text{width}), \text{ square foils} \\ D(\text{diameter}), \text{ round foils} \end{cases} \quad (1)$$

where edge effects have been neglected.

Equivalence Relationships

As previously mentioned, two equivalence relationships are needed to directly apply the Dunn approximation to pin activities. The first, establishing a cylindrical equivalent to β/t, is obtained using mean chord length arguments; the second, obtaining explicitly the cylindrical equivalent to the slab thickness t, is obtained primarily using self-shielding arguments.

β/t Equivalence

The mean chord lengths for infinite slabs and cylinders are, respectively:

$$\bar{\ell}^{w}_{slab} = 2t \quad (2)$$

$$\text{and } \bar{\ell}^{\infty}_{cyl} = 2r. \quad (3)$$

If the ratio of these mean chord lengths is defined as C_∞, then

$$C_w \equiv \frac{\bar{\ell}^{w}_{slab}}{\bar{\ell}^{w}_{cyl}} = \frac{t}{r} \quad (4)$$

Keeping this definition in mind, we will consider both round and square foils, since β can refer to either.

Square Foils

The mean chord lengths for finite slabs (square foils) and cylinders (pins) are, respectively:

$$\bar{\ell}_{slab} = \frac{4t\,L^2}{2L^2 + 4Lt} = \frac{2t}{1 + \frac{2t}{L}} \tag{5}$$

where L is the width and t the thickness,

$$\text{and } \bar{\ell}_{cyl} = \frac{4\pi r^2 h}{2\pi rh + 2\pi r^2} = \frac{2r}{1 + \frac{r}{h}} \tag{6}$$

where h is the height and r the radius.

If the ratio of the finite mean chord lengths is now defined as C, then

$$C \equiv \frac{\bar{\ell}_{slab}}{\bar{\ell}_{cyl}} = \frac{t}{r}\left[\frac{1 + \frac{r}{h}}{1 + \frac{2t}{L}}\right]. \tag{7}$$

In the limit as h and L go to infinity, C becomes C_∞. If r/h and 2t/L are both small, C_∞ can be used as a reasonable approximation to C. Therefore, replacing C by C_∞ in Equation (7) and solving for L/t results in

$$\frac{L}{t} = \frac{2h}{r}. \tag{8}$$

Round Foils

The mean chord length for a disk of diameter D and thickness t is

$$\bar{\ell}_{disk} = \frac{4t\,\pi\,(D/2)^2}{2\pi\,(D/2)^2 + 2\pi\,(D/2)t} = \frac{2t}{1 + \frac{2t}{D}}. \tag{9}$$

If $\bar{\ell}_{disk}$ is used instead of $\bar{\ell}_{slab}$ in an expression similar to Equation (7), i.e.,

$$C' \equiv \frac{t}{r}\left[\frac{1 + \frac{r}{h}}{1 + \frac{2t}{D}}\right], \tag{10}$$

and if, as before, C' is approximated by C_∞ (C_∞ remains unchanged since $\bar{\ell}^\infty_{disk} = \bar{\ell}^\infty_{slab}$), the resulting equation can be solved for D/t, giving

$$\frac{D}{t} = \frac{2h}{r} \cdot \tag{11}$$

The RHS of Equation (11) is the same as the RHS of Equation (8), so for a given thickness, D is equivalent to L. This is the same assumption Dunn used. Therefore, the first equivalence says

$$\frac{\beta}{t} = \frac{2h}{r} \cdot \tag{12}$$

Foil Thickness Equivalence

For small τ ($\tau \equiv \bar{\ell}_\infty \Sigma_t/2$), the self-shielding factors for infinite slabs and cylinders emersed in an isotropic flux can be approximated (neglecting scattering effects) as follows:(3)

$$f_{cyl} \simeq 1 - \frac{1}{2}\tau_{cyl}\left[\frac{8}{3} - \tau_{cyl}\left(\ln \tau_{cyl} + 1.365931\right)\right] \tag{13}$$

$$f_{slab} \simeq 1 - \frac{1}{2}\tau_{slab}\left[.922784 - \ln \tau_{slab} + \frac{1}{3}\tau_{slab}\right] \tag{14}$$

where $\tau_{slab} = t\Sigma_t^{foil}$ and $\tau_{cyl} = r\Sigma_t^{foil}$. Therefore, given an infinite cylinder of radius r, the equivalent thickness, t, of an infinite slab of the same material, which gives the same self shielding factor as the cylinder, can be found by simply equating Equations (13) and (14). The resulting expression

$$\tau_{cyl}\left[\frac{8}{3} - \tau_{cyl}\left(\ln \tau_{cyl} + 1.365931\right)\right]$$

$$= \tau_{slab}\left[.922784 - \ln \qquad + \frac{1}{3}\tau_{slab}\right] \tag{15}$$

also holds true if the usual scattering correction[4] is made to the self-shielding factors

$$f_{corr} = \frac{f_o}{1 - C\,(1 - f_o)} \tag{16}$$

where $C = (\Sigma_s/\Sigma_t)^{foil}$. Equating the corrected self-shielding factors, i.e.,

$$\frac{f_{cyl}}{1 - C\,(1 - f_{cyl})} = \frac{f_{slab}}{1 - C\,(1 - f_{slab})} \tag{17}$$

and using Equations (13) and (14), respectively, for f_{cyl} and f_{slab}, results identically in Equation (15). Equation (15) could be solved by iteration for τ_{slab} and hence t except that the resulting thickness would refer to an equivalent infinite slab instead of a finite one. For this reason a slightly different approach is used. Equations (13) and (14) are assumed to also hold for finite slabs and cylinders, which is in keeping with our previous assumptions of small r/h and 2t/L. Equations (13) through (15) are, therefore, unchanged except for the definition of τ which would be

$$\tau = \frac{1}{2}\,\bar{\ell}\Sigma_t. \tag{18}$$

More specifically,

$$\tau_{cyl} = \frac{r\Sigma_t^{pin}}{1 + \frac{r}{h}} \tag{19}$$

$$\text{and } \tau_{slab} = \frac{t\Sigma_t^{pin}}{1 + \frac{2t}{\beta}} \tag{20}$$

Substituting our first equivalence, Equation (12) into Equation (20) gives

$$\tau_{slab} = \frac{t\Sigma_t^{pin}}{1 + \frac{r}{h}} \tag{21}$$

Solving Equation (21) for t results in our second equivalence expression

$$t = \frac{\left(1 + \frac{r}{h}\right) \tau_{slab}}{\Sigma_t^{pin}} \tag{22}$$

Pin Activity Correction

The desired result (an approximate flux peaking or dipping correction for pin shaped foils) is obtained by substituting Equations (12) and (22) into Equation (1), which then becomes

$$\left(\frac{A_o}{A}\right)_{pin} = 1 - \left(\frac{\Sigma_a^{med} - \Sigma_a^{pin}}{\Sigma_t^{pin}}\right) \tau_{slab} \left(1 + \frac{r}{h}\right) \ln\left(\frac{2h}{r}\right) \tag{23}$$

Finally, the following summarizes the simple procedure leading to A_{pin}^{corr}:

1. Determine Σ_a^{pin}, Σ_t^{pin}, and Σ_a^{med}.
2. Calculate τ_{cyl} from Equation (19).

3. Calculate the LHS of Equation (15) and then solve for τ_{slab} by iteration.
4. Calculate $(A_o/A)_{pin}$ from Equation (23).
5. Correct the measured activity via $A_{pin}^{corr} = A_{pin}^{meas.} (A_o/A)_{pin}$.

Added Comments

Since the results here are based on monoenergetic considerations, Equation (23) actually expresses the energy dependent ratio of the unperturbed to the perturbed flux, $\phi_o(E)/\phi(E)$. The proper spectrum weighted form of Equation (23) can be shown to be

$$\frac{A_o}{A} = \left[\left\langle \frac{1}{1 - \left(1 + \frac{r}{h}\right) \ln \left(\frac{2h}{r}\right) \beta(E)} \right\rangle^{act} \right]^{-1} \qquad (24)$$

where $\left\langle \frac{1}{1 - 1 + \frac{r}{h}) \ln \left(\frac{2h}{r}\right) \beta(E)} \right\rangle^{act}$

$$= \int \left[\frac{1 - \left(1 + \frac{r}{h}\right) \ln \left(\frac{2h}{r}\right) \beta(E) \right]^{-1} \phi^{med}(E) \, \Sigma_{act}^{pin}(E) \, dE}{\int \phi^{med}(E) \, \Sigma_{act}^{pin}(E) \, dE} \qquad (25)$$

and $\beta(E) \equiv \frac{\tau_{slab}(E)}{\Sigma_t^{pin}(E)} / (\Sigma^{med}(E) - \Sigma_a^{pin}(E))$. (26)

For estimating purposes, the simple five step procedure can be retained by using unperturbed spectrum average cross sections.

REFERENCES

1. F. E. Dunn. "Flux Dipping and Peaking in Foils Used in Thermal Disadvantage-Factor Measurements," Trans. Am. Nucl. Soc., vol. 9, no. 1, pp. 189-190. June 1966.

2. D. F. Newman. PCTR Measurements of k for Uranium Lithium Supercells, BNWL-622. Battelle-Northwest, Richland, Washington, December 20, 1967.

3. K. M. Case, F. deHoffman, and G. Plaezek. Introduction to the Theory of Neutron Diffusion Vol. I, U. S. Government Printing Office, Washington, D.C., 1953.

4. N. C. Francis, J. C. Stewart, L. S. Bohl, and T. I. Kreiger. Progress in Nuclear Energy, Pergamon Press, Inc., New York, 1959, Series 1, vol. 3: Physics and Mathematics.

BATCH CORE BURNUP DATA

R. P. Matsen

Destructive analysis data from samples cut from PRTR rods have been received, plotted for consistency checks, and processed through the ISODIL burnup analysis code. Twenty-four samples were cut from rods extracted from the reactor during the first, second, and third interim shutdowns. When the basic data were received from analytical chemistry, it was plotted in order to discover inaccurate measurements. A much lower percentage of these inaccurate measurements exists among this data than for any set received to date. The few questionable results were submitted for reanalysis. In addition, several samples of unirradiated fuel have been submitted for analysis in order to ensure that the data for the zero burnup point is as reliable as that from the other samples.

Results from the ISODIL code reveal that the maximum sample exposure was approximately 9000 MWd/MTM for (as expected) a sample cut from the middle of a replaceable rod taken from a ring-one element during the third interim shutdown.* Input data for a least squares burnup analysis code BUFIT was

* See R. P. Matsen's "Program BUFIT: A Least Squares Code for the Analysis of Burnup Data" in this report.

punched via the ISODIL code for fourteen samples taken from replaceable rods that were irradiated in ring three of the core. The least squares analysis of this data, in order to extract cross section ratio information, has begun.

PRTR BATCH CORE - CRITICAL TEST NO. 4

J. H. Lauby and L. D. Williams

The fourth interim critical tests were conducted on the 55 fuel-element Batch Core loading at the PRTR at an average core burnup of 5330 MWd/MTM. Tests were also conducted on two smaller loadings of 31 and 19 fuel elements. Moderator level worth measurements were made using critical approach and positive period techniques. Data were obtained at three different moderator levels (100, 95, and 90 in.) for each of the loadings. Reactor oscillator measurements were also made for each configuration at the high moderator level.

The ^{10}B concentrations for each critical configuration were determined by reactivity comparisons made in the Thermal Test Reactor (TTR) using standard samples. Analysis of the ^{10}B concentration measurements is in progress.

Moderator level reactivity coefficients for each loading and boron concentration were consistent with previous measurements. Critical moderator height and one-standard deviation uncertainties for each critical loading were determined from the positive period measurements using program LEARN. Final analysis of the moderator level reactivity coefficients and critical moderator height is awaiting the ^{10}B results.

Analysis of the reactor oscillator experiments is complete. The results of measurements of β/ℓ, the ratio of the delayed neutron fraction to the prompt neutron lifetime, are summarized in Table 2.7 as a function of burnup for the Batch Core experiment.

TABLE 2.7. The Results of Measurements of β/ℓ

Average Core Burnup, MWd/MTM	Core Size, Fuel Elements	^{10}B Conc., wppm ^{10}B	β/ℓ, sec^{-1}
0	55	20.4	17.9 ± 0.5
~10	77 (250 watt)	21.8	20 ± 1
~10	77 (1 MW)	22.5	18.1 ± 0.9
3560	55	13.8	15.1 ± 0.6
5330	55	10.6	14.3 ± 0.3
6139	31	5.9	10.4 ± 0.5
6512	19	2.3	8.0 ± 0.2

3.0 FUELS TECHNOLOGY

PRTR HIGH POWER DENSITY FUEL EVALUATIONS

M. D. Freshley and T. B. Burley

Mixed-oxide fuels have been irradiated in PRTR as part of the Batch Core Experiment (BCE) to significant burnups at power generations greater than those employed in commercial power reactors. Actual peak linear power generations were approximately 20 kW/ft with maximum fuel temperatures (about 2600 °C) near melting. Peak burnups are approximately 11,000 MWd/MTM. Although the majority of the 66 High Power Density nineteen-rod cluster fuel elements included in the Batch Core Experiment were vibrationally compacted powder fuel, pellet fuel fabricated by both the hot-pressed and the cold-pressed-sintered processes was included. Detailed post-irradiation examination of selected elements and rods from the BCE is being conducted to evaluate the irradiation performance of the different fuel types. A summary of the elements and rods from the BCE selected for detailed examination is provided in Table 3.1.

Three elements (Fe-6065, 6520, and 6700) as indicated in Table 3.1 were thoroughly examined in the PRTR basin to assess their condition. In general, the visual examination indicates that the condition of the elements is excellent (Figures 3.1 through 3.9).

Varying amounts of a loosely adhering or flakey, reddish-brown appearing crud has formed on the surfaces of the elements as a result of operation in the neutral pH coolant in PRTR. The crud deposits, which were heaviest on the heat transfer surfaces of the rods, had a spotty appearance in some instances (Figure 3.2) whereas the thicker appearing deposits were more uniform (Figure 3.5). Thicker, non-uniform deposits are associated with localized turbulence on non-heat transfer surfaces

TABLE 3.1. Summary of Elements and Rods from the Batch Core Experiment Selected for Detailed Postirradiation Evaluation

Element Number	Rod No.	Fuel Type	Estimated Peak Burnup, MWd/MTM	Profilometer Scan	Gamma Scan
6065[a]	FE-74	VP,[d] UO_2-2 wt% PuO_2	10,000	x	x
	FD-17	↓		x	x
	FS-07	↓		x	x
6519	#2[c]	VP, UO_2-2 wt% PuO_2	4,600		
	FR-72	↓		x	x
	#4[c]	↓			
6520[a]	#8[c]	VP, UO_2-2 wt% PuO_2	11,000		
	FR-78	↓		x	x
	#7[c]	↓			
6700[a]	A-14	HP,[e] UO_2-2 wt% PuO_2	9,600	x	
	A-103	CPS,[f] UO_2-2 wt% PuO_2		x	
	A-102	CPS, UO_2-2 wt% PuO_2		x	x
6701	A-23	HP, UO_2-2 wt% PuO_2	3,800	x	x
	A-12	HP, UO_2-2 wt% PuO_2			
FERTF[b]	FS-41	VP, UO_2-2 wt% PuO_2	Low	x	
	FS-42	↓	↓	x	
	FS-43	↓	↓	x	
	FS-45	↓	↓	x	
	FS-46	↓	↓	x	
	FS-48	↓	↓	x	

a. Elements selected for underwater examination before disassembly.
b. Rods irradiated to low burnup under identical conditions in the Fuel Element Rupture Test Facility in PRTR.
c. Rods instrumented to monitor internal gas pressure and plenum gas temperature during irradiation.
d. VP refers to vibrationally compacted.
e. HP refers to hot-pressed pellet fuel.
f. CPS refers to cold-pressed-sintered pellet fuel.

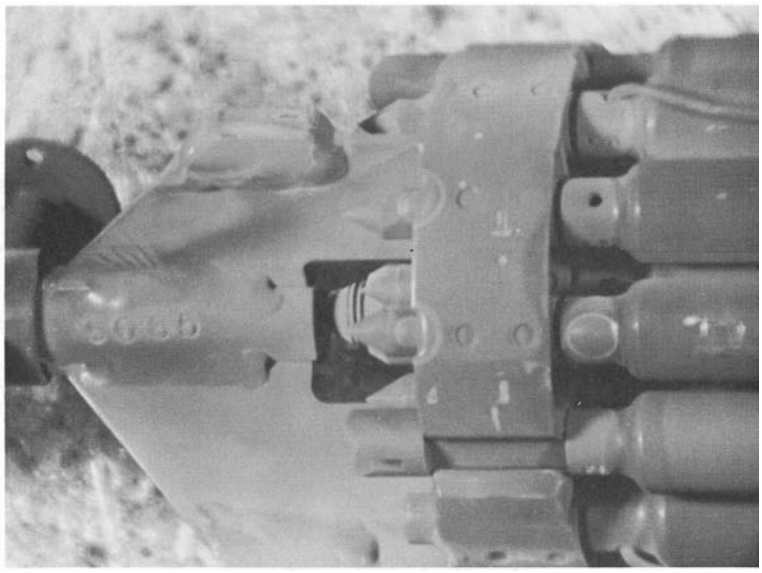

6065-2

FIGURE 3.1. Top End Bracket Region of PRTR FE-6065 Showing the Position of One Replaceable Rod and Small Amounts of White Zirconium Oxide Corrosion Associated with the Fission Welds on the Spiral Wire Wraps and the Rod Pin Weld on the End Bracket

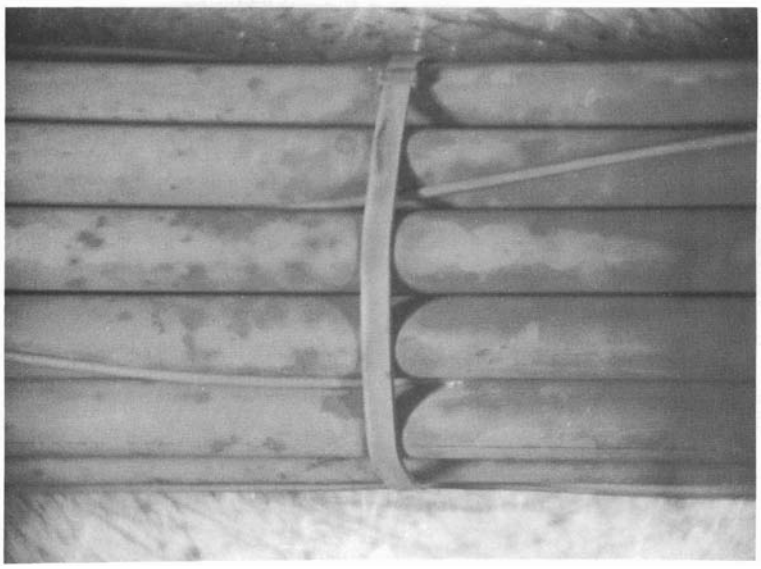

6065-13

FIGURE 3.2. Fuel Rod Region of PRTR FE-6065 Showing Spotty Crud Deposit and a Circumferential Strip Band

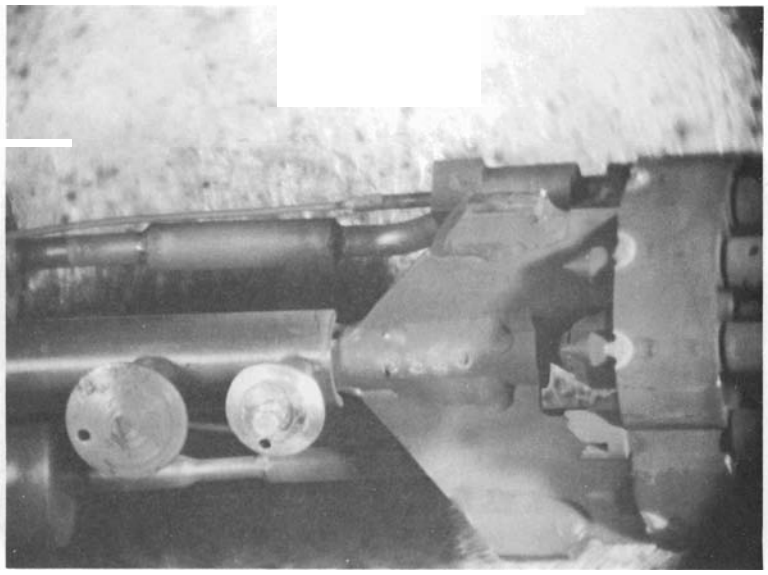

6520-3

FIGURE 3.3. Top End Bracket Region of PRTR FE-6520 Showing the Piping Associated with the Instrumented Rods and a Small Amount of White Zirconium Oxide Corrosion on the Rod Pin Fission Welds

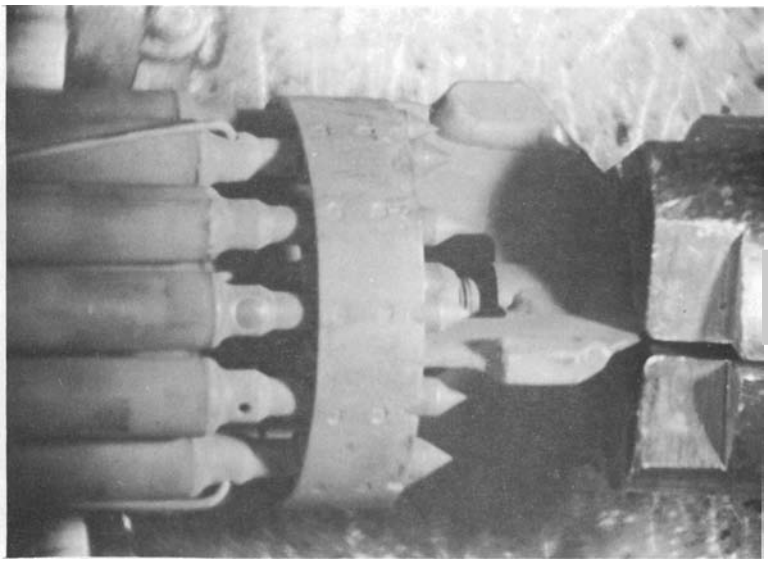

6520-19

FIGURE 3.4. Bottom End Bracket Region of PRTR FE-6520

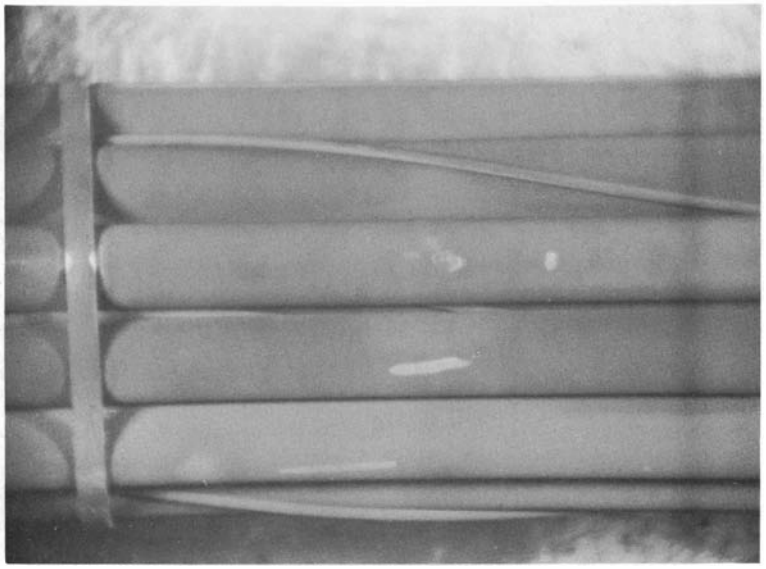

6520-11

FIGURE 3.5. *Fuel Rod Region of PRTR FE-6520 Showing Appearance of Uniform Crud Deposit (White areas are scuff marks.)*

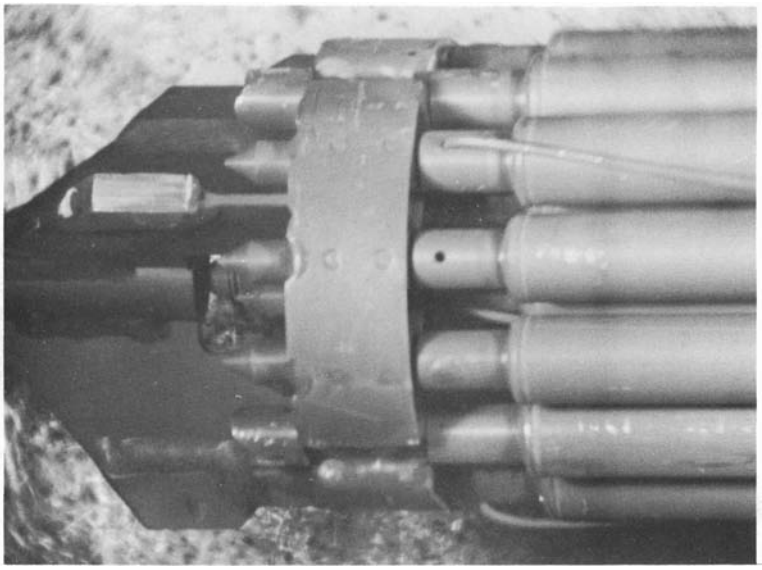

6700-1

FIGURE 3.6. *Top End Bracket Region of PRTR FE-6700 Showing Axial Abrasion Marks on the Wear Pads*

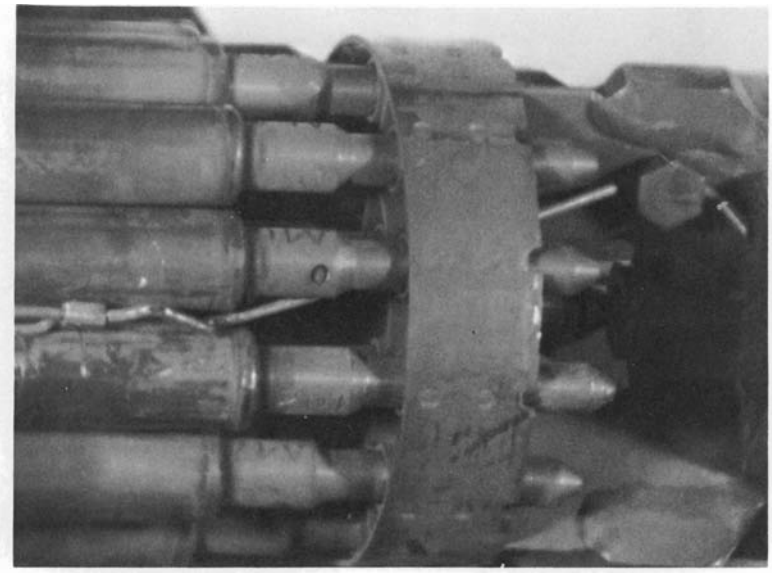

6700-11

FIGURE 3.7. *Bottom End Bracket Region of PRTR FE-6700 Showing the Broken Spiral Wire Wrap that Was Spliced Remotely in the Basin (The wire fractured at the bend in the end plug.)*

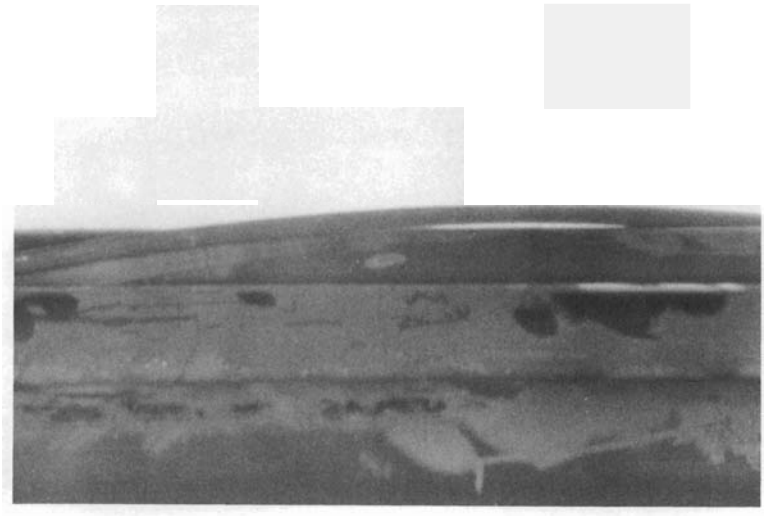

6700-6

FIGURE 3.8. *Fuel Rod Region of PRTR FE-6700 Showing a Loose Spiral Wire Wrap*

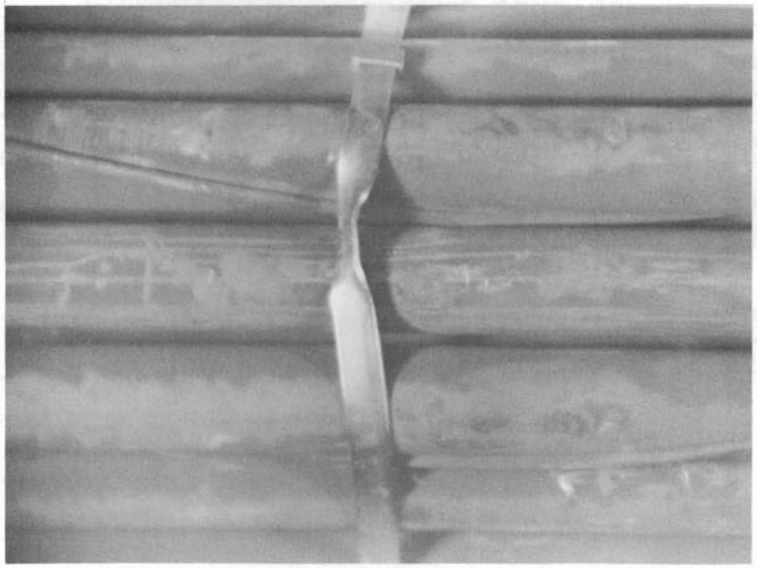

6700-8

FIGURE 3.9. *Fuel* **Rod Region of PRTR FE-6700 Showing** *Typical* **Damage to a** *Circumferential* **Strip Band Caused by Snagging During Charge-Discharge**

such as end brackets. The general amount of crud deposition on individual elements varied depending upon the position of the element in the core, i.e., heavier crud deposits appeared to have formed on elements that were located in the lower flux regions of the core. Crud deposition was also heavier in the lower flux regions near the ends of individual elements. On some elements, the crud was noticeably heavier on the side of the element that probably faced away from the center of the reactor. The thickness and type of crud deposits evident on PRTR fuel element surfaces are not similar to deposits that have been associated with measurable effects on fuel cladding heat transfer or fuel channel pressure drop. The possible effects of the crud deposits on fuel performance will be investigated more thoroughly during the detailed destructive examination of the rods.

Small amounts of white zirconium oxide corrosion were associated with the spot fusion welds where the spiral wire wraps are attached to the end plugs and where the fuel rod pins are attached to the end brackets (Figures 3.1 and 3.3). The small amount of accelerated corrosion in these localized areas, which was probably caused by impure cover gas during welding, did not affect fuel performance.

Fractured spiral wire wraps which were spliced remotely performed satisfactorily during continued irradiation (Figure 3.7).

Damaged circumferential strip bands caused by snagging during charge-discharge operations were observed on some elements (Figure 3.9). It was necessary to periodically replace broken strip bands to permit continued irradiation of the elements in PRTR.

Some of the spiral wound spacer wires loosened on element FE-6700 which contained hot-pressed pellet fuel (Figure 3.8). No loose wires were observed on vibrationally compacted fuel rods. The loosening is probably the result of rod shortening caused by core-clad interaction or creep induced by differential thermal expansion between the wire and the fuel rods. There was no evidence of fretting corrosion or crud removal associated with the loose wires, thus indicating that the wires are probably tight during operation.

The selected fuel rods are now being removed from the elements for gamma and profilometer scanning prior to commencing the detailed destructive examination in Radiometallurgy.

The detailed postirradiation examination of seventeen ceramographic specimens from seven vibrationally compacted UO_2-PuO_2 fuel rods removed from the PRTR core following Interim Critical Test No. 6 was completed and the results are being analyzed. Peak burnups on the rods ranged from 3000 to

9000 MWd/MTM and peak linear rod power generations ranged from 5 to 18 kW/ft. Preliminary evaluation of the data indicates good correlations between fission gas release fraction and fuel temperature and between the fuel structures formed during irradiation and rod power. None of the apparent anomalies in the fuel structure-rod power relationship, such as those which have been observed in low burnup vibrationally compacted fuel rods, were indicated in these higher burnup rods. This indicates that time-temperature dependent diffusion processes provide more uniform and consistent structural features in vibrationally compacted UO_2-PuO_2 fuels during extended irradiation. Comparison of the burnup data as determined by the Nd and Cs methods shows that Cs burnup values are lower than the Nd values in the central regions of the high power rods and higher than the Nd values in the end regions. These results illustrate the axial migration of Cs from the higher to the lower fuel temperature regions within a rod.

PRTR EXTENDED BURNUP FUEL EVALUATIONS

M. D. Freshley and T. B. Burley

A variety of experimental UO_2 and UO_2-PuO_2 elements containing 0.5, 1.0, and 2.0 wt% PuO_2 were irradiated in PRTR fringe positions during the Batch Core Experiment. The purpose of these irradiations was to obtain information on the performance of selected pre-Batch Core vintage elements subjected to extended burnup. Some of the fringe elements have been undergoing irradiation in the PRTR since startup of the reactor in 1961 and have operated at advanced linear rod power generations projected for light water reactors now being committed. A summary of representative elements and rods selected for detailed postirradiation evaluation of fuel performance is presented in Table 3.2.

TABLE 3.2. Summary of Extended Burnup Elements and Rods from Fringe Positions of the PRTR Selected for Detailed Postirradiation Evaluation

Element Number	Rod No.	Fuel Type	Estimated Peak Burnup, MWd/MTM	Profilometer Scan	Gamma Scan
1037[a]	(?)	SW,[d] UO_2	14,500		X
	(?)	SW,[d] UO_2			
5118[a]	DB-63	VP,[e] MM,[f] UO_2-0.5 wt% PuO_2	18,500		x
	DA-48	VP,[e] MM,[f] UO_2-0.5 wt% PuO_2			
5186	ZZ-17	CPS,[g] UO_2-0.5 wt% PuO_2	12,500		x
	ZZ-7	t			x
	ZZ-12				x
	CN-5	SW, MM, UO_2-0.5 wt% PuO_2			
5224[a]	CS-27	SW, MM, UO_2-0.5 wt% PuO_2	13,500		x
5226[a]	DF-80	VP, PI,[h] UO_2-1.0 wt% PuO_2	11,500		x
6003[a]	5C-27	VP, PI, UO_2-2 wt% PuO_2	13,000	x	x
6005[a]	5F-36	SW, PI, UO_2-2 wt% PuO_2	8,000	x	x
6521	#6[c]	VP, PI, ThO_2-5 wt% PuO_2	Low		x
6500[b]	SC	VP, SC, UO_2-2 wt% PuO_2	1,800		

a. Elements selected for underwater examination before disassembly.
b. Two rods containing salt cycle reprocessed fuel material are included in this element.
c. This rod was instrumented to monitor internal gas pressure and plenum gas pressure during irradiation.
d. SW refers to swage compacted fuel rods.
e. VP refers to vibrationally comp'acted fuel rods.
f. MM refers to heterogeneously enriched or incrementally loaded fuel material.
g. CPS refers to cold-pressed-sintered pellet fuel.
h. PI refers to high-energy-rate pneumatically impacted fuel.

Six elements (FE-1037, 5118, 5224, 5226, 6003, and 6005), as indicated in Table 3.2, were examined in the PRTR basin to assess their condition before disassembly operations commenced. In general, the visual examination indicated that the condition of the elements was excellent (Figures 3.10 through 3.22). The observations made on particular aspects of the condition of the elements were similar to those made on the Batch Core Experiment elements examined.

Crud deposition was generally heavier on these elements, which were located in the lower flux fringe positions of the core, as illustrated in the figures. However, the thickness of the crud was not judged sufficient to affect fuel cladding heat transfer or fuel channel pressure drop.

Fretting corrosion occurred because the initial PRTR fuel element design did not provide extended surface contact areas between the end brackets and the pressure tubes. Clip-on extended surface area wear pads were remotely attached to the end brackets of elements of this design (Figures 3.13 and 3.14). These clip-on pads have performed satisfactorily and process tube wear was eliminated.

PRTR primary coolant was initially controlled at pH-9 with LiOH. As power generation and surface heat flux was increased, crevice corrosion at the contact points between the fuel rods and the circumferential strip bands occurred (Figure 3.16). The maximum depth of cladding penetration measured in the peak heat flux region of a rod was 4.5 mils or 16% of the wall thickness. Since it was recognized that the corrosion rate would increase in the crevices as surface heat flux was increased, the coolant was operated at neutral pH to avoid the corrosion problem and the old circumferential strip bands on the elements were replaced. Although the crevice corrosion occurred early in the irradiation of the elements and did not continue in neutral pH coolant, evidence of the localized attack remains on the rod surfaces of some elements.

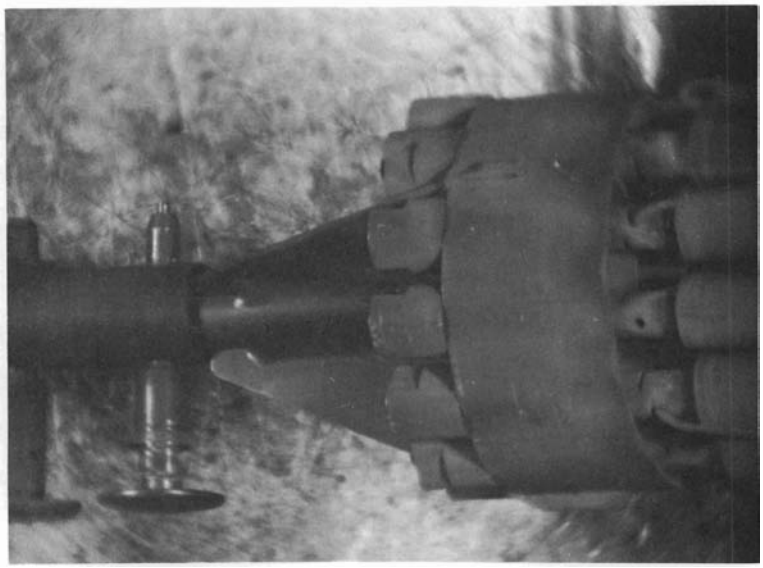

1037-3

FIGURE 3.10. Top End Bracket Region of PRTR FE-1037

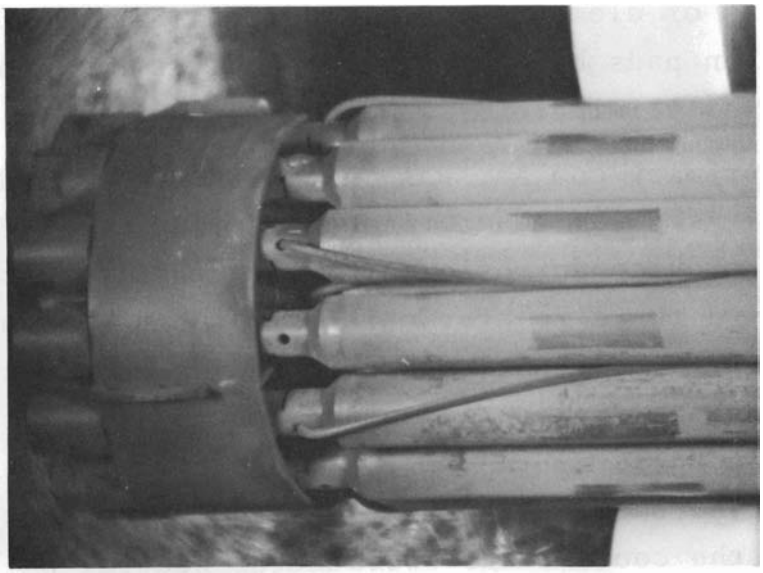

1037-6

FIGURE 3.11. Top End Bracket Region of PRTR FE-1037 Showing Attachment of Spiral Spacing Wires and Crud Deposition. Crud deposit has been removed by contact with the rollers on the Fuel Examination Tray.

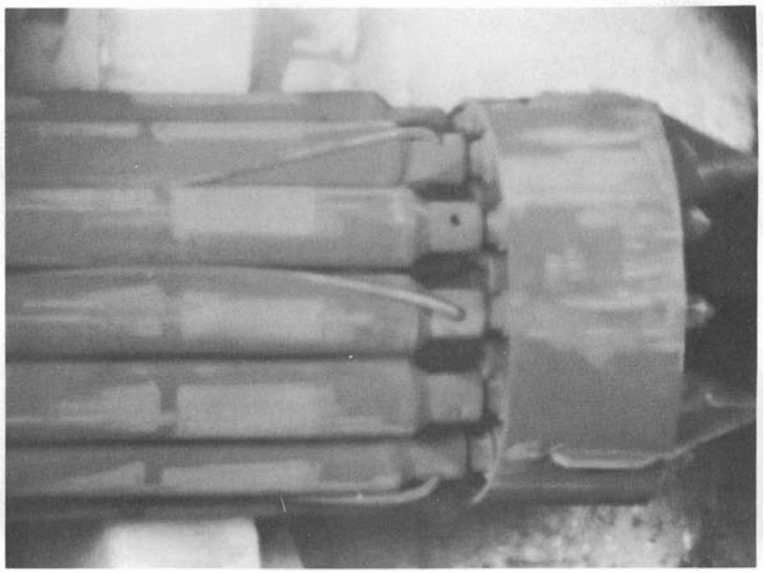

1037-16

FIGURE 3.12. Bottom End Bracket Region of PRTR FE-2037 Showing Heavy Crud Deposit. Crud is easily removed by scuffing during fuel handling.

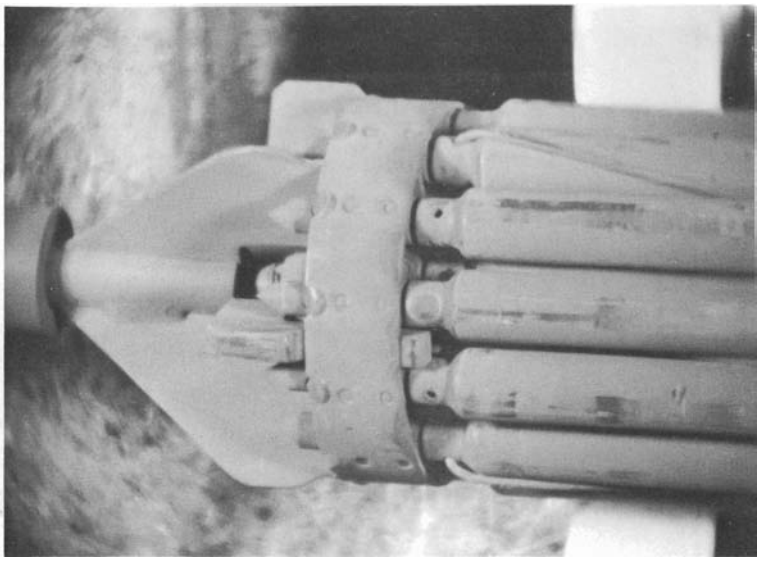

5118-20

FIGURE 3.23. Top End Bracket Region of PRTR FE-5118 Heavy Crud Deposit and Clip-on Extended Surface Area Wear Pads that Were Remotely Attached to the End Bracket During the Early Part of the Irradiation

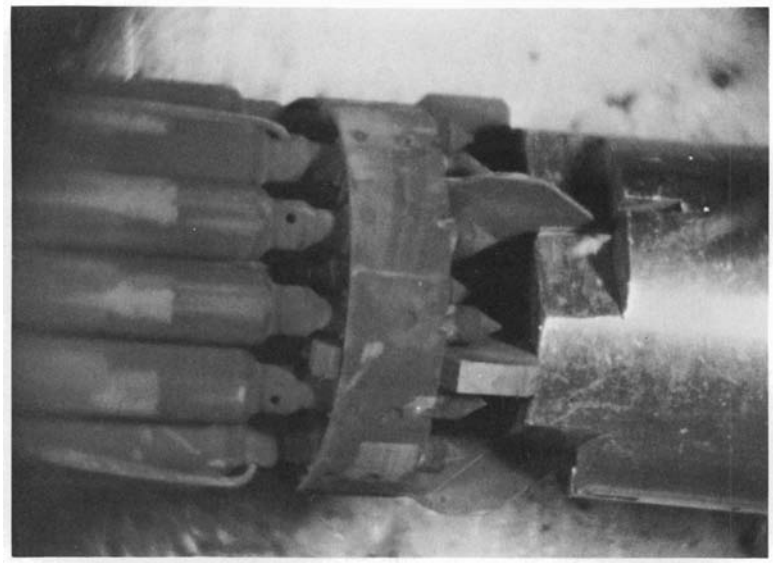

5118-3

FIGURE 3.14. *Bottom End Bracket Region of PRTR FE-5118 Showing Heavy Crud Deposit and Clip-on Extended Surface Wear Pads*

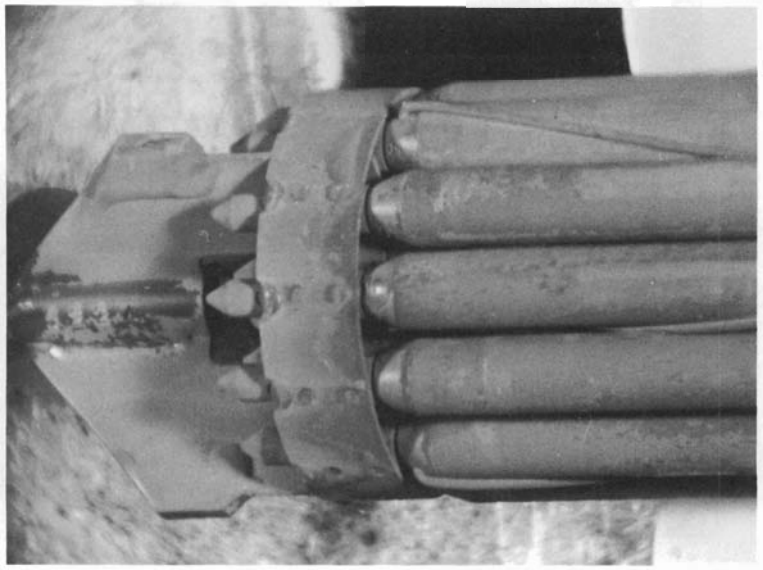

5224-4

FIGURE 3.25. *Top End Bracket of PRTR FE-5224 Showing Variations in Crud Deposition Associated with End Bracket Turbulence*

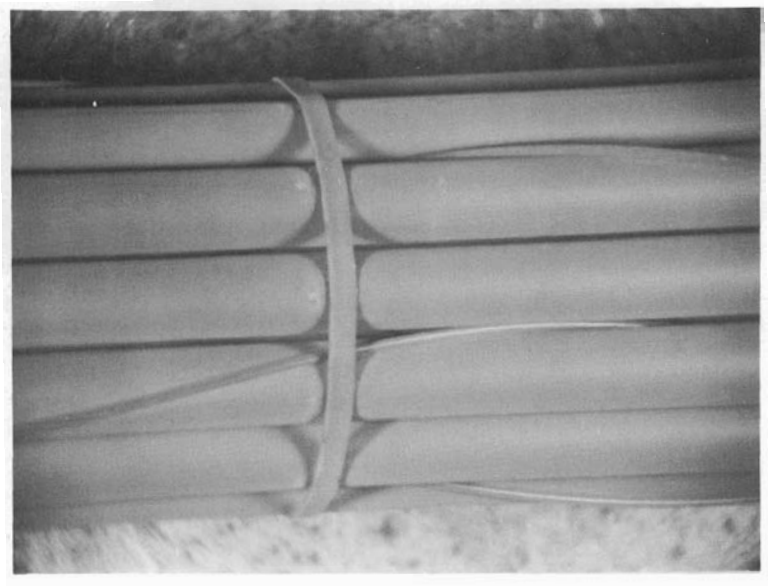

5224-6

FIGURE 3.16. Fuel Rod Region of PRTR FE-5224 Showing Uniform Crud Deposition and the Crevice Corrosion on the Rod Surfaces Associated with the Circumferential Strip Bands that Occurred During Operation with LiOH-Controlled pH-9 Coolant

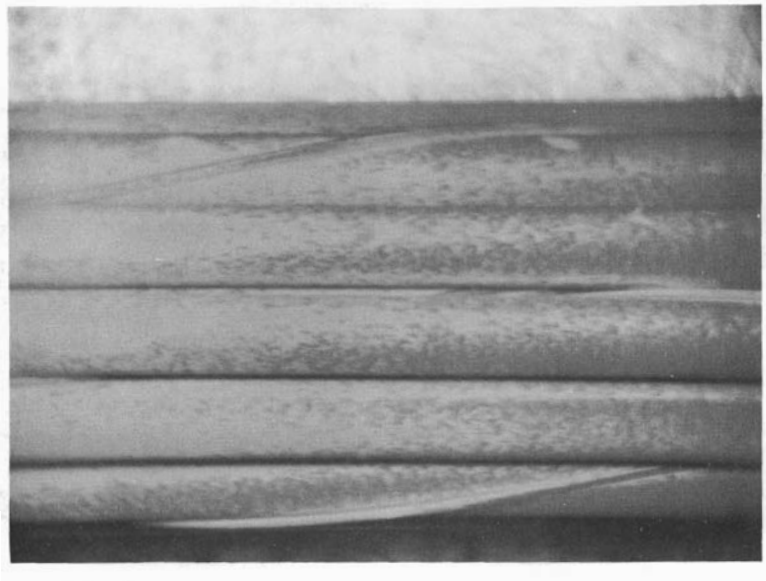

5224-11

FIGURE 3.17. Fuel Rod Region Near the Bottom of PRTR FE-5224 Showing Spotty or Speckled Crud Deposition in the Transition Region from a Light to Heavier Deposit

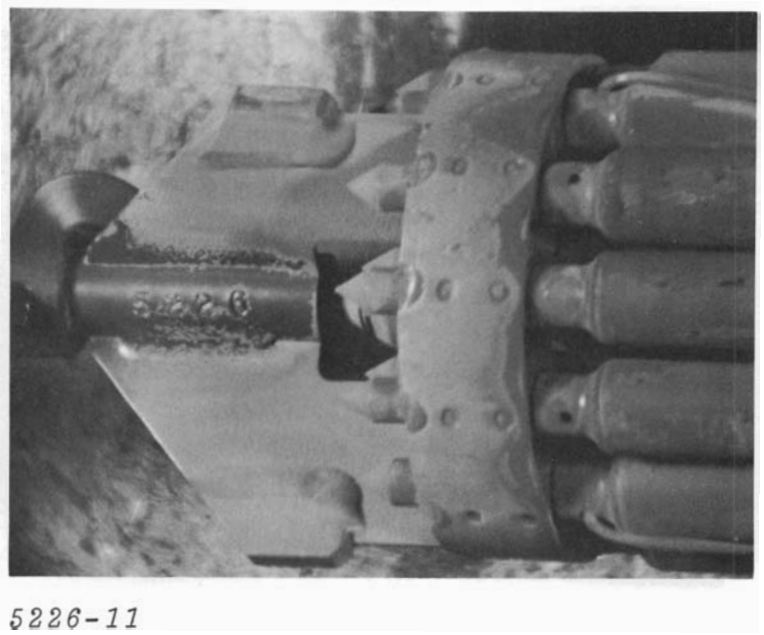

FIGURE 3.18. *Top End Bracket Region of PRTR FE-5226 Showing Variations in Crud Deposition Associated with End Bracket Turbulence*

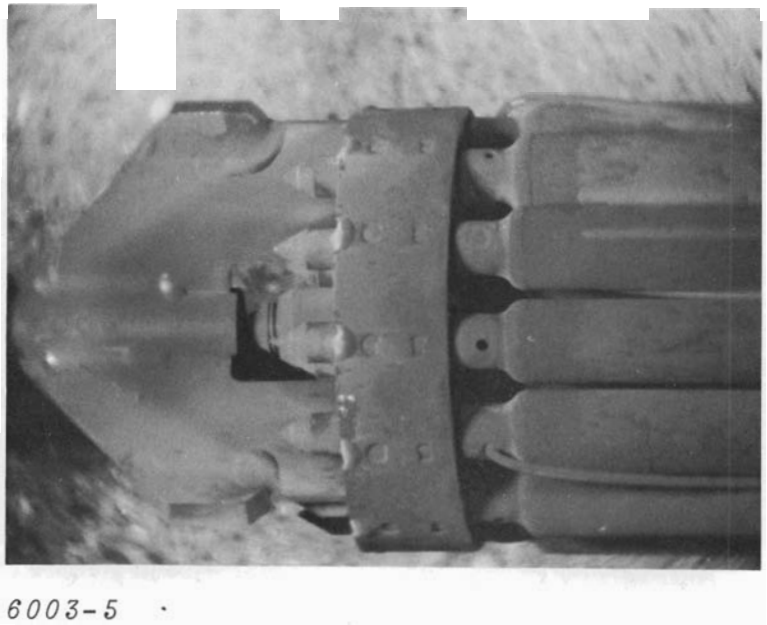

FIGURE 3.19. *Top End Bracket Region of PRTR FE-6003 Showing Change in the Appearance of the Crud Deposit on the Rod Surfaces at the End Plug-to-Fuel Interface*

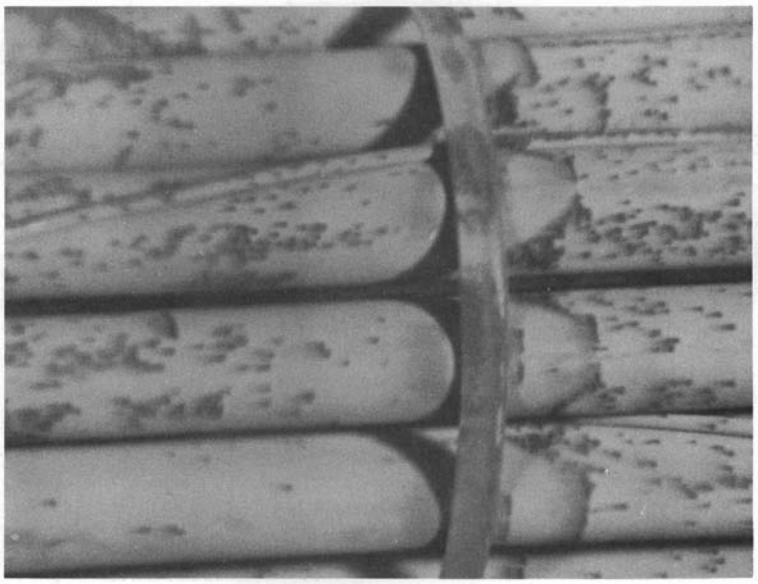

6003-15

FIGURE 3.20. *Fuel Rod Region of PRTR FE-6003 Showing Spotty Crud Deposition*

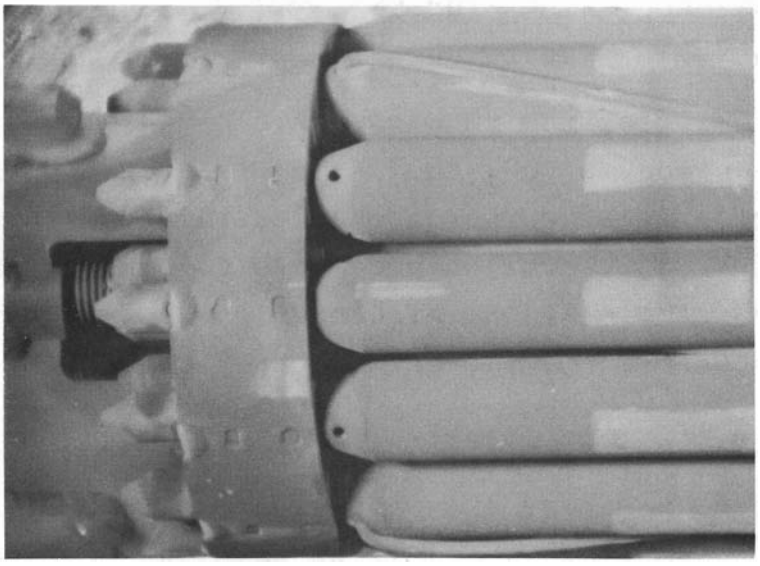

6005-4

FIGURE 3.21. *Top End Bracket Region of PRTR FE-6005*

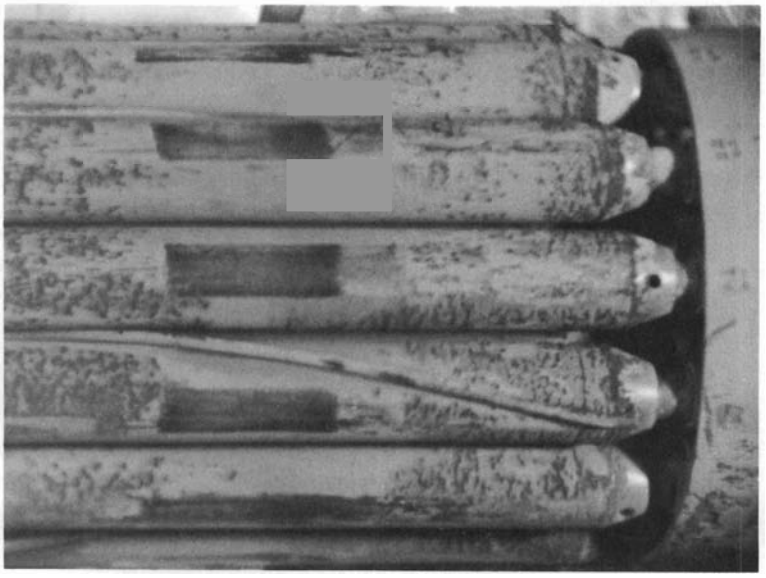

6005-17

FIGURE 3.22. Bottom End Bracket Region of PRTR FE-6005 Showing Spotty Crud Deposits. The loose crud deposit has been removed by contact with the rollers on the Fuel Examination Tray.

HIGH EXPOSURE PLUTONIUM STUDIES

R. C. Smith, L. G. Faust, and H. H. Van Tuyl

Measurement of the electromagnetic radiations from a Yankee high exposure PuO_2 fuel sample is continuing. This sample represents a "worse case" situation for surface dose rate from currently available commercial power reactor plutonium. The sample is the highest exposure plutonium specimen obtained to date in sufficient quantity to permit extensive surface dose rate measurements. The dose rate, as measured through 33 mils of plastic on the 36,000 MWd/MTM burnup sample, is summarized in Table 3.3. The greatest rate of increase, which occurred during the first 60 days, was caused by the formation of short half life ^{237}U as it built up to an equilibrium concentration. The major contributor to the reduced rate of increase after considerable time following separation is the ^{241}Am formation.

TABLE 3.3. Measured Surface Dose Rate Through 33 Mils of Plastic from a Yankee High Exposure PuO_2 Sample (36,000 MWd/MTM)

Days Since Separation	Surface Dose Rate, rad/hr
1	4.8
58	5.9
116	6.1
160	6.5
365 (a)	7.9 (a)

a. *Calculated Value*

Data is also being obtained on a high exposure Dresden sample with a burnup of approximately 30,000 MWd/MTM. The dose rate for this sample, as calculated by PUSHLD, is summarized in Table 3.4. The calculated dose rate for the Yankee sample after 1 year is approximately 7.9 rad/hr.

TABLE 3.4. Calculated Surface Dose Rate from a Dresden High Exposure Plutonium Sample (30,000 MWd/MTM)

Days Since Separation	Surface Dose Rate, rad/hr
1	3.5
100	5.2
365	7.5

Dose rates for the various plutonium samples are sensitive to the isotopic contents which are compared in Table 3.5. The isotopic content of these samples is not entirely representative of what would be formed in current design PWR's and BWR's. Although the Yankee sample, with the higher ^{238}Pu content, has the higher dose rate for the first few years, calculations indicate that the surface dose rate for the two samples approaches the same value of 18.4 rad/hr 5 years after chemical separation.

TABLE 3.5. Comparison of Isotopic Compositions of Yankee and Dresden Plutonium

Pu Source	Burnup, MWd/MTM	Isotopic Content, wt% ^{238}Pu	^{239}Pu	^{240}Pu	^{241}Pu	^{242}Pu
Yankee	36,000	1.92	63.3	19.2	11.68	3.88
Dresden	30,000	1.44	52.9	27.7	12.10	5.77

A computer study now underway indicates that the early Yankee reactor parameters may provide a "worst case" situation from the standpoint of radiation from single recycle plutonium. Preliminary data from the study also indicates that the isotopic composition of plutonium from present and planned PWR's and BWR's will be more nearly the same and the gamma surface dose rate will be less severe.

DEFECT TESTING

M. D. Freshley and T. B. Burley

As fuel operating conditions approach inherent performance limits, defect behavior becomes increasingly important and may ultimately prove to be the limiting performance factor. Because reactors cannot operate economically without accommodating defective fuel rods, satisfactory defect behavior must be demonstrated under high performance conditions before widespread acceptance of mixed oxide fuels can be expected. It is therefore important to determine the behavior characteristics and operating limits for defective fuel and, in particular, the effects of specific power, burnup, and fuel form on defective fuel behavior.

Irradiation tests of defected and nondefected oxide fuels will be performed under high performance conditions in the ETR M-3 loop facility. The defect testing program includes variations of three important parameters: 1) fuel form (solid pellet, cored pellet); 2) power generation (22 to 27 kW/ft); and 3) burnup.

Defect tests will be performed at nominal peak linear rod power generations of 22 and 27 kW/ft. Testing at about 22 kW/ft is expected to produce maximum fuel temperatures (2600 to 2800 °C) near melting in pellet containing rods, and tests at 27 kW/ft will produce moderate fuel melting. Most of the tests will be performed at about 22 kW/ft because the conditions are similar to the maximum conditions projected for light water reactors now being committed and are considered to be in a critical surface heat flux region (500,000 Btu/hr-ft^2) for defect fuel performance.

The performance data to be derived include rod dimensional changes, fuel washout, waterlogging, fission gas and fission product release, fuel rod swelling, stoichiometry changes and their effect on fuel performance.

Modification of the ETR M-3 loop facility to accommodate defect tests is in progress and the test element design is being scoped. The test element will probably be a nineteen-rod cluster design with the defected rods located in replaceable positions in the outer twelve-rod ring. A sleeve will surround the element to protect the pressure tube from possible damage. The nondefected, nonreplaceable rods in the test element will incorporate various fuel design parameters for evaluation such as: solid pellet fuel, cored pellet fuel, different diametral gaps, and different cladding surface treatments. Tests are expected to commence during the first part of next year.

INSTRUMENTED FUEL TESTS

M. D. Freshley, T. B. Burley, and F. E. Panisko

Vibrationally compacted UO_2-PuO_2 fuel rods instrumented to monitor internal gas pressure during irradiation were successfully irradiated in PRTR to determine the effects of fuel temperature and burnup on both sorbed and fission gas release.

Although some information was obtained on the fission gas release mechanisms involved, the experiments were not specifically designed for this purpose. An experiment more suitably designed to study gas release mechanisms for cold-pressed-sintered pellet and vibrationally compacted UO_2-PuO_2 fuel during irradiation to extended burnup is being scoped for irradiation in the ATR.

Temperatures normally associated with specific structural features in UO_2-PuO_2 fuels during irradiation are used in the postirradiation evaluation of fuel performance. An assembly composed of rods containing cold-pressed-sintered and vibrationally compacted UO_2-PuO_2 fuel will be instrumented with thermocouples to monitor fuel temperatures during programmed power increases and during steady-state operation in the ETR M-3 loop. The thermal characteristics to be studied include in-reactor sintering and grain growth kinetics, grain growth temperatures, comparative effective thermal conductivities of the different fuel types, and fuel-to-clad heat transfer coefficients. These experimentally determined parameters obtained by direct measurement will aid in understanding fuel behavior.

4.0 REACTOR SAFETY

ZODIAC-ALTHAEA COMPARISON WITH Pu ENRICHED FUELS

E. T. Merrill, E. A. Schnaible

A comparison was made between the results of burnup calculations obtained using the ZODIAC G[1] and ALTHAEA[2] codes. The ALTHAEA code uses a simplified model for spectral averaging cross sections and as a result uses only about 1/400 of the computing time required for a corresponding ZODIAC G solution. There are numerous burnup calculations required in the studies of using plutonium in a typical boiling water reactor (Oyster Creek). Thus, there is a considerable savings realized in using ALTHAEA rather than ZODIAC G for these studies.

A comparison of ZODIAC and ALTHAEA calculations covering three different plutonium enriched fuels is shown in Table 4.1. For each fuel the reactivity and concentrations of uranium and plutonium isotopes are compared at three fuel exposures. The adjustable parameters in the ALTHAEA code were set at the same values for all fuels. The comparison showed that isotopic concentrations agreed within 1% with the exception of the ^{242}Pu concentration in the low density fuel. Values of k_∞ checked within 0.5% for all exposures and all fuels calculated. As a result of this comparison, we have concluded that the ALTHAEA code can be used in studies of reactor operation and behavior for plutonium-fueled cores as well as uranium-fueled cores.

POWER DISTRIBUTION CALCULATIONS IN OYSTER CREEK FUEL ASSEMBLIES USING URANIUM AND PLUTONIUM

J. N. Morgan, R. E. Shaver

Plutonium loadings for an Oyster Creek assembly have been chosen so that the rod peak-to-average power is less than that in the original uranium-only fuel. The plutonium loadings use the same uranium enrichments as in the initial Oyster Creek fuel assembly plus two plutonium fuel enrichments. In the plutonium fuel assembly 50% of the rods contain natural uranium

TABLE 4.1. Zodiac-Althaea Comparison

		Exposure MWD/MT	K_∞	Isotope Concentration, g/MT ^{235}U	^{218}U	Total Pu	^{293}Pu	^{240}Pu	^{241}Pu	^{242}Pu
Enrichment 3.6 wt %	ZODIAC	4,000	1.095	6,313.0	949,958.0	39,317.2	22,446.2	10,139.5	5,014.4	1,717.2
	% Variation		0.27	0.02	-0.001	-0.02	-0.08	-0.03	0.21	0.10
	ZODIAC	8,000	1.079	5,827.8	947,252.0	38,041.4	20,755.3	10,047.7	5,421.5	1,816.9
	% Variation		0.27	0.01	-0.002	-0.01	-0.11	-0.14	0.49	0.30
	ZODIAC	10,786	1.069	5,501.5	945,336.0	37,161.1	19,669.5	9,952.3	5,642.0	1,897.3
	% Variation		0.19	0.01	0.001	-0.01	-0.12	-0.28	0.68	0.50
Enrichment 2.7 wt %	ZODIAC	4,000	1.075	6,249.2	962,321.0	27,000.1	15,171.7	7,071.0	3,523.7	1,233.7
	% Variation		-0.19	0.02	-0.000	0.07	0.13	0.13	-0.26	-0.09
	ZODIAC	8,000	1.054	5,622.5	959,436.0	26,117.7	13,839.8	7,069.4	3,843.3	1,365.2
	% Variation		-0.28	0.06	-0.004	0.20	0.38	0.13	-0.25	-0.05
	ZODIAC	10,777	1.041	5,208.6	957,375.0	25,523.7	13,026.2	7,028.1	4,001.8	1,467.6
	% Variation		-0.48	-0.08	-0.006	0.28	0.55	0.06	-0.17	0.07
Enrichment 4.3 wt %	ZODIAC	4,000	1.130	3,927.1	603,219.0	30,481.2	16,858.4	8,162.6	4,041.9	1,418.3
	% Variation		-0.18	0.07	-0.004	0.05	-0.06	0.18	0.04	0.50
Low fuel density	ZODIAC	8,000	1.104	3,533.3	601,087.0	28,637.0	14,613.4	8,096.7	4,364.7	1,562.2
			-0.27	0.08	-0.010	0.16	0.01	0.20	0.24	1.13
	ZODIAC	10,748	1.086	3,269.4	599,581.0	27,389.2	13,217.7	7,988.1	4,506.1	1,677.3
	% Variation		-0.28	0.10	-.015	0.27	0.14	0.12	0.36	1.65

enriched with plutonium. This represents approximately twice as much plutonium per assembly as would normally be discharged in a spent uranium assembly.

The power distribution and enrichment patterns are shown in Figure 4.1 for the reference Oyster Creek fuel assembly. The enrichments and power distribution for the plutonium loading fuel assembly is noted in Figure 4.2. The maximum rod power is 1.18 in the plutonium-enriched assemblies, whereas the maximum rod peak in the uranium assembly is 1.19. Using this reference assembly, the change in reactivity with void fraction was determined for no control, operating temperature conditions.

FLARE calculations will be carried out for the plutonium assembly and results compared with those from the previous uranium-only first core analysis to assist in determining any differences that may have safety implications.

Enrichment Distribution

P					P	P
						P
						P
						P
					P	P
P				P	P	X
P	P	P	P	P	X	X

X **1.19** w/o **uranium**

P **1.67** w/o **uranium**

2.42 w/o **uranium**

Average fissile/rod
2.10 w/o

Power Distribution[a] **(32% voids)**

0.99	1.13	1.07	1.06	1.12	0.95	1.19
1.13	0.95	0.90	0.89	0.94	1.12	1.07
1.07	0.90	0.84	0.84	0.89	1.06	1.03
1.06	0.89	0.84	0.85	0.90	1.07	1.04
1.12	0.94	0.89	0.90	0.96	0.87	1.10
0.95	1.12	1.06	1.07	0.87	0.98	0.91
1.19	1.07	1.03	1.04	1.10	0.91	1.08

(a) *Average* ***power per rod in fuel*** *assembly equals 1.00.*

FIGURE 4.2. *Initial* ***Oyster Creek*** *Uranium Loading*

Enrichment Distribution

	E_1	E_1			P	P
E_1	E_2	E_2	E_2	E_2		P
E_1	E_2	E_2	E_2	E_2	E_1	P
	E_2	E_2	E_2	E_1	E_1	P
	E_2	E_2	E_1	E_1		P
P		E_1	E_1		P	X
P	P	P	P	P	X	X

[X] **1.19** w/o **uranium**

[P] **1.67** w/o **uranium**

2.42 w/o **uranium**

[E_1] **1.06** w/o **Pu fissile in nat. U**

[E_2] **1.385** w/o **Pu fissile in nat. U**

Average fissile/Rod **1.91** w/o

Power Distribution[a] **(32% voids)**

1.01	1.10	1.04	0.85	0.97	0.92	1.17
1.10	1.00	0.92	0.97	1.14	0.98	1.03
1.04	0.92	0.83	0.85	0.99	1.16	0.96
0.85	0.97	0.85	0.87	0.90	1.18	0.97
0.97	1.14	0.99	0.90	1.05	1.01	1.05
0.92	0.98	1.16	1.18	1.01	0.96	0.91
1.17	1.03	0.96	0.97	1.05	0.91	1.09

Pu Composition, w/o

239	240	241	242
.60	.25	.11	.04

[a] *Average power per rod in fuel assembly equals 1.00.*

FIGURE 4.2. *Initial Oyster* ***Creek*** *Plutonium-Uranium Loading*

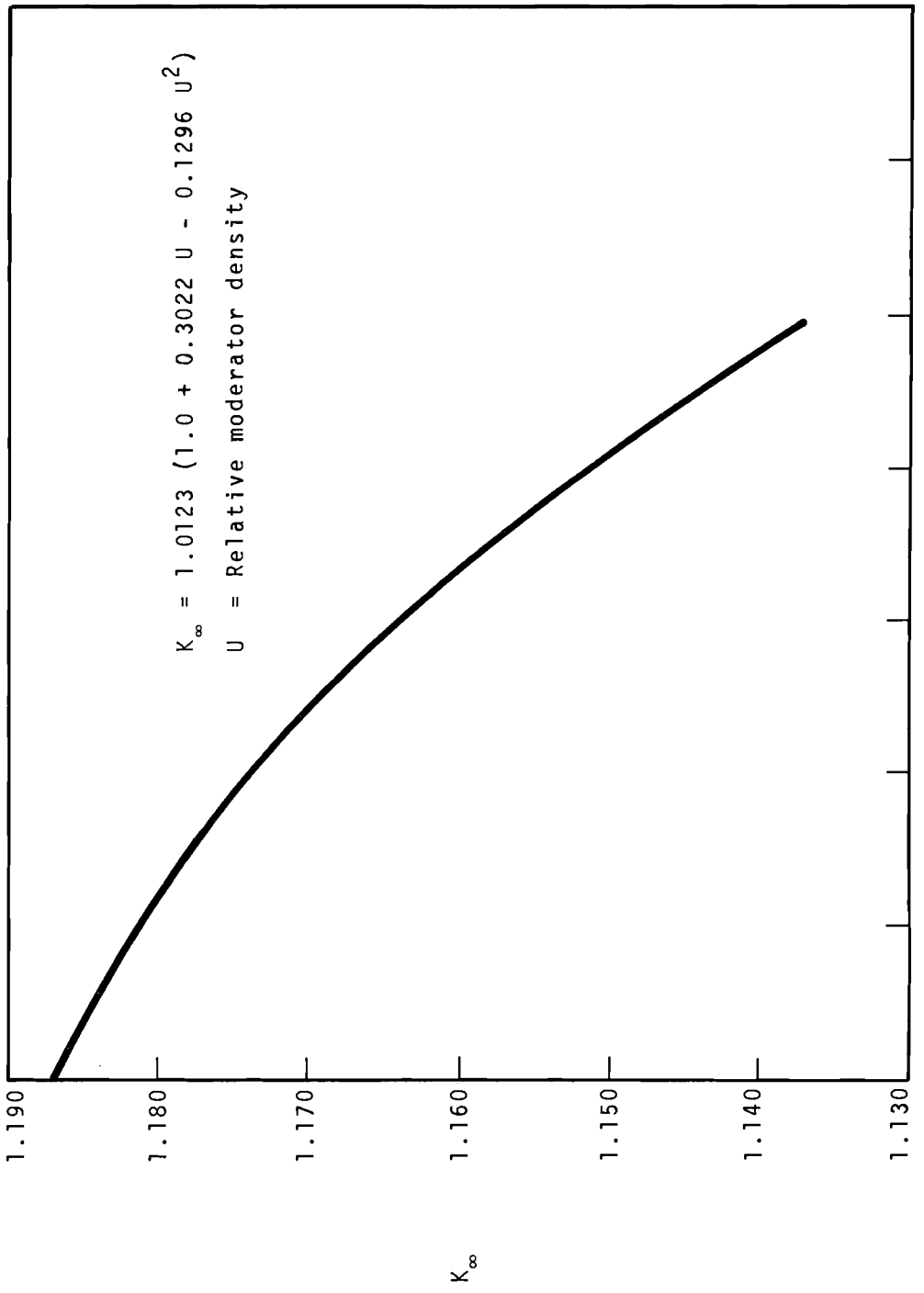

FIGURE 4.3 *Oyster Creek Simulation (Plutonium Loading at Startup, Operation Temperature, No Control) 2DB K_∞ Versus Void*

TRANSIENT TESTING

M. D. Freshley and T. B. Burley

A knowledge of the behavior of reactor fuels subjected to high energy, short duration power excursions is essential to permit a complete appraisal of fuel performance and reactor safety. The transient behavior of mixed-oxide fuels is being investigated to determine if there are special considerations associated with adding PuO_2 enrichment to UO_2 fuels that would influence power reactor operation. Some of the specific objectives of the transient testing program are to:

- Compare the transient behavior of pelleted and vibrationally compacted UO_2 and UO_2-PuO_2 fuels
- Establish fuel failure thresholds, modes of failure, and possible failure consequences
- Investigate the extent of metal-water reaction, the magnitude and nature of pressure pulses generated, the fraction of thermal energy converted to mechanical energy, the chemical reactivity of the dispersed fuel, and the extent of fission gas release
- Investigate the effects of PuO_2 particle size
- Investigate the effects of different transient conditions
- Investigate the effects of various preirradiation conditions.

A joint program involving Pacific Northwest Laboratory, General Electric Company, and Idaho Nuclear Corporation designed to investigate the transient behavior of mixed-oxide thermal reactor fuels in SPERT is being formulated. The purpose of the cooperative PNL/GE/INC effort is to investigate the possible effects of adding PuO_2 enrichment to UO_2 fuels in different ways. Although a complete program designed to study PuO_2 particle size effects in UO_2-PuO_2 cold-pressed-sintered pellet fuel involving approximately 25 transient irradiations was

outlined, the first test series involves 4 or 5 irradiations to investigate the possible effect of single 500 μm diam. PuO_2 particles strategically positioned in enriched UO_2 pellets. The Zircaloy-clad pins will be tested at three different energy levels in SPERT. These irradiation tests will be supported by detailed preirradiation characterization and postirradiation evaluation of the fuel pins. Subsequent test series will involve investigation of the transient behavior of pins containing multiple PuO_2 particles and pins preirradiated under different conditions.

A joint program involving Pacific Northwest Laboratory and Argonne National Laboratory is being conducted to compare the transient behavior of pelleted and vibrationally compacted fuels by irradiations in the transparent vessel in TREAT. Detailed evaluation of high speed motion pictures permit studies of the failure modes and failure thresholds of the different fuel types.

A few experiments will be conducted in the transparent vessel in TREAT with pins designed to eliminate power peaking at the ends of the fuel column. The purpose of these tests is to confirm previous comparative results with cold-pressed-sintered pellet and vibrationally compacted fuel pins in which there was considerable power peaking in the end regions.

Seven Zircaloy-clad pins containing UO_2 fuel (4.79% ^{235}U) are being fabricated for these confirmative experiments. Two of the seven pins which contain cold-pressed-sintered pellet fuel, will be used for calibration purposes to determine the axial power profile. Three of the remaining five pins will contain pellet fuel and two, vibrationally compacted powder fuel.

Hafnium wafers (0.100-in. thick) were placed at each end of the 5.5-in. fuel column in the first calibration capsule to suppress power peaking in the end regions and provide a more prototypic axial power distribution during transient irradiation. Gamma activity measurements made on individual pellets

after irradiation in TREAT indicate that the power peaking was reduced but that the power in the end regions was still approximately 5 and 7% higher than the average activation of the fuel column (Figure 4.4).

Another calibration capsule was fabricated with additional hafnium absorber material (0.200-in. thick) at each end of the fuel column and is awaiting irradiation in TREAT.

REFERENCES

1. D. D. Matsumoto and R. H. Holeman, "ZODIAC-G," Reactor Physics Department Technical Activities Quarterly Report, January, February, March 1968, BNWL-775. Battelle-Northwest, Richland, Washington, July 1968.

2. E. T. Merrill. Unpublished Data. Battelle-Northwest, Richland, Washington. (Preliminary Data: ALTHAEA, Part I-A, One-Dimensional Two-Group Diffusion Code with an Effective Four-Group Burnup.)

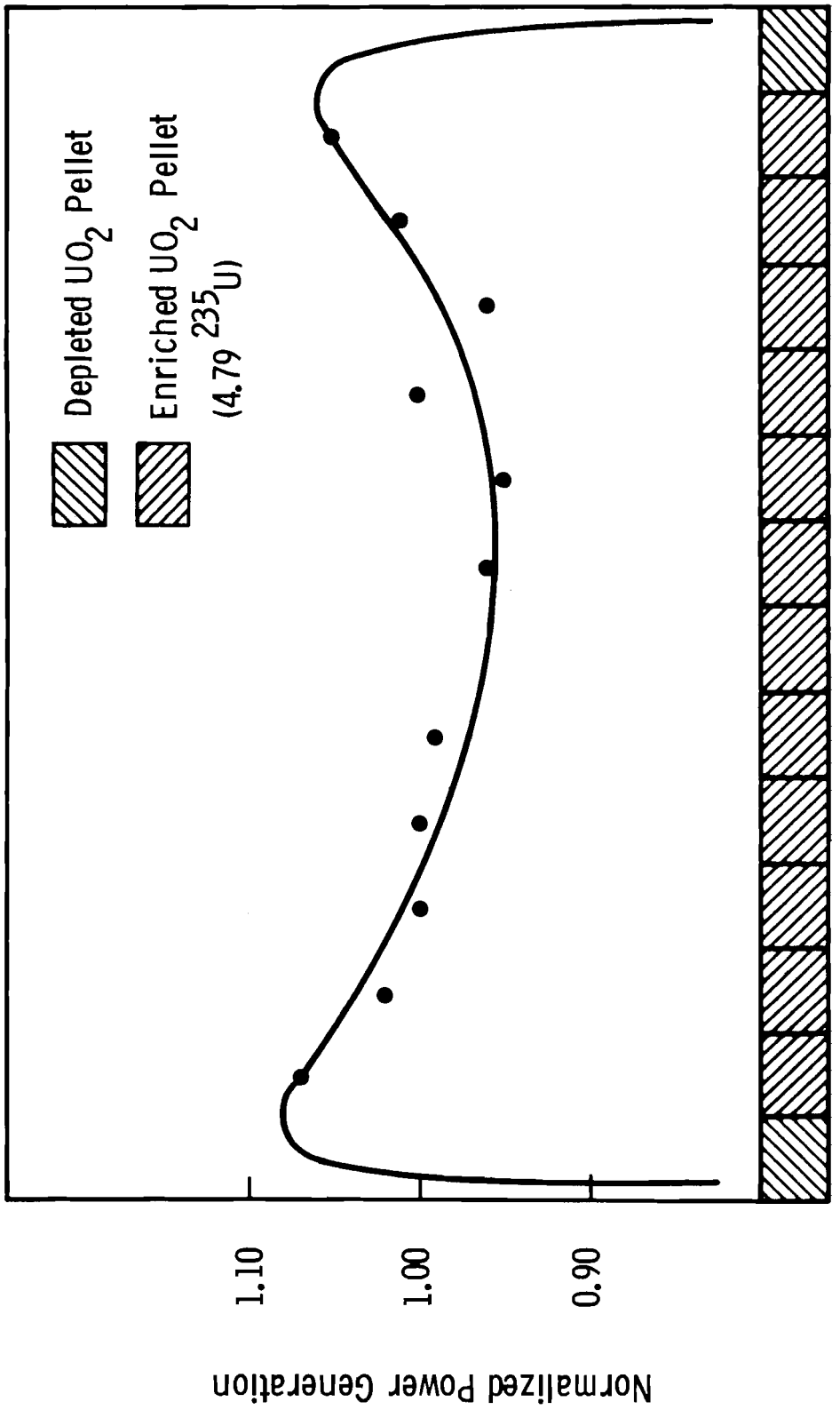

FIGURE 4.4. Measured Axial Power Profile in a TREAT Calibration Capsule (MDF-1) Which Contained an 0.00 in Thick Hafnium Absorber Disc at Each End of the 5.5 in. Long Enriched UO_2 Fuel Column

5.0 PLUTONIUM RECYCLE TEST REACTOR

REACTOR OPERATIONS

R. F. Warnick

During the early part of the report period, efforts were directed toward resuming reactor operation. The primary coolant system was filled with heavy water and hydrostatically pressure tested to 1875 psig. The reactor was fueled with the 55-element batch core and the fourth series of interim critical tests was completed. Then, the decision was made to deactivate the PRTR. The balance of the report period was spent draining and drying the coolant systems and deactivating the reactor equipment.

All the heavy water has been drained from the primary and moderator coolant systems and the primary system has been dried. The out-of-reactor portion of the moderator coolant system has been dried. The following have been drained and dried: the reflector coolant system, the rotating shield coolant system, the lower access space cooling lines, the primary pressurization portion of the helium system, the FERTF makeup system, the FERTF light water injection system, the filtered water line, the sanitary water lines inside the containment vessel, the emergency water lines and the process water lines inside the containment vessel. Draining and drying of all other coolant systems are in progress.

PROCESS TECHNOLOGY

R. H. Purcell

The fourth interim critical tests were successfully completed for the 55 fuel element batch core and two, smaller loadings; 31 and 19 fuel elements. Moderator level worth measurements were made using subcritical approach and positive period techniques. Data were obtained at three different moderator levels (100 in., 95 in., and 90 in.) for each loading. Reactor

oscillator measurements were also made for each configuration at the higher moderator level. Moderator archive samples were taken for each critical configuration such that the boron concentrations can be determined at a later date.

The PRTR Annual Safety Report for CY1968 was approved and issued.

6.0 PUBLICATIONS AND PRESENTATIONS

PUBLICATIONS

R. P. Matsen. An Analysis of Yankee-Rowe Burnup Data, BNWL-1122. Battelle-Northwest, Richland, Washington, July 1969.

PRESENTATIONS

R. C. Liikala, J. L. Carter, Jr., S. R. Dwivedi, G. L. Gelhaus and V. G. Uotinen. "Uncertainties in the Analysis of Plutonium Fueled Assemblies," Trans. Am. Nucl. Soc., vol. 12, no. 1, pp. 227-228.

B. R. Leonard, Jr., "Thermal Cross Sections of Plutonium Isotopes and the 1968-1969 IAEA Review," Trans. Am. Nucl. Soc., vol. 12, no. 1, pp. 226-227.

D. E. Christensen and E. S. Murphy. "Analysis of Nuclear Fuel by Gamma Scanning," Trans. Am. Nucl. Soc., vol. 12, no. 1, pp. 93-94.

R. P. Matsen, G. J. Busselman, R. H. Holeman and R. C. Liikala. "Analysis of Uranium Fuel Irradiated in Yankee Reactor," Trans. Am. Nucl. Soc., vol. 12, no. 1, pp. 31-32.

ACCEPTED FOR PRESENTATION

V. O. Uotinen, J. H. Lauby, W. P. Stinson (BNW), and S. R. Dwivedi (India). Measured and Calculated β/ℓ for Some Uniform H_2O Lattices, to be presented at the American Nuclear Society Wznter Meeting in San Francisco, California, November 30 to December 4, 1969.

D. H. Thomsen. Analytical Studies of One and Two-Dimensional Cell Representations for Cluster Geometry Fuels, to be presented at the American Nuclear Society Winter Meeting in San Francisco, California, November 30 to December 4, 1969.

DISTRIBUTION

No. of Copies

OFFSITE

1 AEC Chicago Patent Group

G. H. Lee

9 AEC Division of Reactor Development and Technology

G. Boyer
A. Giambusso
W. H. Hannum
J. Kruth
W. H. Layman
M. Shaw
J. Simmons
E. E. Sinclair
M. J. Whitman

214 AEC Division of Technical Information Extension

3 Argonne National Laboratory

R. Avery
C. H. Bean
R. E. Machery

1 Babcock and Wilcox

H. M. Jones

1 Brookhaven National Laboratory

J. Chernick

3 Combustion Engineering

W. P. Chernock
R. Harding
S. Visner

1 CNEN - Centro Studi-Nucleaire
Casaccia, Rome, Italy

Ugo Farinelli

2 E. I. du Pont deNemours & Co., Inc., SRL

G. Dessauer
H. Honeck

No. of Copies

1 ENEL
Via G. B. Martini
(Pizaaz Verdi)
Rome, Italy

Mr. Paoletti Gualandi

3 General Electric Co., San Jose

D. L. Fischer
S. Levy
R. B. Richards

2 General Electric Co., Vallecitos Atomic Lab.

B. F. Judson
T. M. Snyder

1 Idaho Nuclear Corporation

D. deBoisblanc

2 Nuclear Materials and Equipment Corp.

C. S. Caldwell
K. Puechl

1 NUKEM
D-645, HANAU
POSTFACH 869
Germany

Mr. Wolgang K. L. Jager

1 Pakistan Institute of Nuclear Sci. & Tech.
P. O. Nilore
Rawalpindi, Pakistan

M. A. Mannan

1 Power Reactor & Nuclear Fuel Development Corp.
9-13, 1-chome, Akasaka,
Minato-ku, Tokyo, Japan

Setsuo Kobayashi

1 S. C. K. - C. E. N.
MOL-DONK
Belgium

Dr. H. Vanden Broeck
BRL.

2 United Nuclear Corporation

T. B. Holden
G. Sofer

No. of Copies

6 Westinghouse Electric Corporation

R. J. French
R. S. Miller
P. M. Murray
R. E. Olsen
J. B. Roll
J. H. Wright

ONSITE - HANFORD

1 AEC Chicago Patent Group

R. K. Sharp (Richland)

4 AEC RDT Site Representative

W. E. Fry
P. G. Holsted (2)
J. B. Kitchen

2 AEC Richland Operations Office

H. A. House
C. L. Robinson

3 Battelle Memorial Institute

8 Douglas United Nuclear

T. W. Ambrose
C. D. Harrington
C. W. Kuhlman
W. S. Nechodom
G. F. Owsley
DUN Files (3)

70 Battelle-Northwest

F. W. Albaugh
C. A. Bennett
S. H. Bush
G. J. Busselman
J. J. Cadwell
D. E. Christensen
F. G. Dawson (10)
D. R. de Halas
D. E. Deonigi
R. L. Dillon
E. A. Eschbach
E. A. Evans
J. R. Fishbaugher
J. C. Fox

No. of Copies

Battelle-Northwest (contd)

M. D. Freshley
G. L. Gelhaus
S. Goldsmith'
W. L. Hampson
R. E. Heineman
H. L. Henry
P. L. Hofmann
U. P. Jenquin
B. M. Johnson
R. A. Kennedy
J. W. Kutcher
J. H. Lauby
B. R. Leonard
R. C. Liikala
C. W. Lindenmeier
R. P. Matsen
D. F. Newman
D. R. Oden
H. M. Parker
L. T. Pedersen
R. H. Purcell
W. L. Purcell
W. D. Richmond
L. C. Schmid
R. C. Smith
R. I. Smith
W. P. Stinson
D. H. Thomsen
L. D. Turner
V. O. Uotinen
A. D. Vaughn
R. G. Wheeler
L. D. Williams
N. G. Wittenbrock
W. C. Wolkenhauer
D. C. Worlton
K. L. Young
F. R. Zaloudek
BNW Legal (2)
Technical Information (5)
Technical Publications (2)